Subregional activity in the dentate gyrus is amplified during elevated cognitive demands

Charlotte C.M. Castillon[1], Shintaro Otsuka[1], John N. Armstrong[1], Anis Contractor[1,2,3]

[1]Department of Neuroscience, [2]Department of Psychiatry and Behavioral Sciences Feinberg School of Medicine, [3]Department of Neurobiology, Weinberg College of Arts and Sciences Northwestern University

Correspondence: Anis Contractor
Dept of Neuroscience
Northwestern University Feinberg School of Medicine
303 E. Chicago Ave
Chicago, Il 60611
a-contractor@northwestern.edu
Tel: 312 503 1843

Words in Abstract – 264 ; Introduction – 483 ; Discussion - 1438

Acknowledgements: We thank members of the Contractor lab for helpful discussion and Ms. Astrid Castellanos for assistance during the performance of this study. This work was supported by NIH/NINDS 5R01NS115471 to AC.

Author Contributions: C.C.M.C., J.N.A., and A.C. designed experiments. C.C.M.C. performed all behavioral testing, immunohistochemistry, imaging and analysis. S.O. developed the touch screen automated task and produced code to operate the procedures. C.C.M.C. and A.C. prepared the manuscript. All authors approved the final version.

Abstract:

Neural activity in the dentate gyrus (DG) is required for the detection and discrimination of novelty, context and patterns, amongst other cognitive processes. Previous studies have shown that granule cell activation differs between the supra and infrapyramidal blades of the DG during a range of hippocampal dependent tasks yet how excitatory dynamics within the DG drive and modulate this blade-specific bias under varying cognitive demands remains unclear.
Here we used an automated touch screen pattern separation task combined to temporally controlled tagging of active neurons to determine how increasing cognitive demand shapes the spatial patterns of activity in the DG. We observed that as task difficulty increased, DG activation became progressively biased toward the suprapyramidal blade, accompanied by structured distributions of active mature granule cells (mGCs) along the apex-to-blade and hilar-to-molecular layer axes. Selective inhibition of mature granule cells (mGCs) did not affect the patterned distribution of active cells but profoundly impaired performance, as mice were no longer able to discriminate between closely spaced locations. In contrast, chemogenetic inhibition of adult-born granule cells (abDGCs) beyond a critical window of their maturation significantly impaired performance of mice during high-demand conditions, elevated overall mGC activity and disrupted the blade-specific distribution of active mGCs even in animals that successfully completed the task. These findings demonstrate how a high cognitive demand pattern separation task preferentially activates mGCs in subregions of the DG and are consistent with a modulatory role for abDGCs on the dentate circuit which in part governs the spatially organized patterns of activity of mGCs.

Introduction:

The dentate gyrus (DG) is the input structure to the hippocampus and plays important roles in episodic memory[1], spatial coding[2], novelty detection[3] as well as in separating patterns[4]. A long-standing proposal stemming from early computational studies, suggest that the DG contribute to pattern separation based on its anatomical connectivity[5-7] . The DG is the gateway to the hippocampus receiving direct excitatory input from the entorhinal cortex (EC). The large number of granule neurons in the DG receiving input from a relatively smaller population of EC has been proposed to promote expansion recoding which, along with sparse firing of granule cells, allows the separation of inputs at the level of neural activity[8].
The granule cell layer of the DG is organized into two blades, termed the suprapyramidal (SB) and infrapyramidal (IB) blades. When viewed in transverse cross-section[9], mature granule cells (mGCs) exhibit asymmetric activation across these blades during hippocampal-dependent

tasks[10-13], with greater activity typically observed in the SB compared to the IB[10-12] However, the circuit-level mechanisms underlying this functional asymmetry remain unresolved.

In addition to mature populations, the subgranular zone (SGZ) of the DG serves as a neurogenic niche where new granule neurons continue to be generated throughout adulthood[14-17]. This process of adult neurogenesis gives rise to adult-born dentate granule cells (abDGCs), which can remodel local circuitry and potentially contribute to memory flexibility[18]. Interestingly, the asymmetry in mGC activation across the blades parallels an asymmetry in neurogenesis, with higher numbers of abDGCs reported in the SB[19-22].

In this study, we investigated whether performance in a cognitively demanding task alters the patterns of neural activity in the dorsal dentate gyrus (DG), and how manipulation of excitatory populations within the DG can modulate these activity patterns. Using TRAP2 mice[23] to label neurons activated during a touchscreen-based spatial discrimination task, we observed a consistent bias in activity between the two blades of the DG. When the cognitive demand of the task was elevated by reducing the degree of spatial separation, there was an increase of TRAP cells activity and a more prominent and amplified spatial bias with active neurons distributed preferentially to the SB and relatively reduced in the IB. To dissect the contribution of distinct excitatory populations, we selectively inhibited either mature or adult-born granule cells during task performance. We found that manipulating these populations had differential effects on the blade-specific bias of activation, indicating distinct roles for mGCs and abDGCs in shaping DG representations during spatial cognition. Inhibition of mature granule cells did not alter the blade bias of activation but markedly impaired performance, as mice were no longer able to discriminate closely spaced locations under high cognitive demand. In contrast, chemogenetic inhibition of abDGCs beyond a critical window of their maturation, decreased task performance, increased overall mGC activity, and reduced the blade-specific bias of activation, suggesting that abDGC activity is required to maintain proper DG network organization under high cognitive load. Together, these findings reinforce the significance of neural activity in the dorsal DG in spatial pattern separation and highlight the circuit contributions of both abDGCs and mGCs to behaviors requiring a high cognitive demand.

Results:

Amplified blade-biased activity of GCs during a high cognitive demand pattern separation task

Prior work has demonstrated that expression of immediate early genes in the DG including Arc [10], c-Fos[12] and Zif268[24] correlate with behavioral state and are active in both mature and young

abDGCs. Genetic strategies using TRAP1 mice[25] and TetTag mice[26,27] have also demonstrated that active GC populations can be labeled with these strategies. To determine whether behaviorally induced labeling of both mGCs and abDGCs is observed in TRAP2 mice (Fos$^{2a\text{-}iCreERT2}$;Ai9) we combined birth-dating of abDGCs with a single exposure to voluntary wheel running which is known to activate DG neurons[25] (Figure S1A). Mice given access to running wheels for 4 hours had elevated numbers of TRAP+ neurons throughout the DG, with both mature and immature neurons labeled (Figure S1B-F). TRAP+ labeling of abDGCs was observed in birth-dated neurons 14 days post injection (dpi) from BrdU (Figure S1E & F). No double labeled TRAP+ BrdU+ neurons were observed in younger neurons prior to this timepoint (Figure S1F). Importantly, an analysis of the blade specific localization of TRAP+ neurons demonstrated that in home cage controls there was a small bias in the distribution of active neurons to the SB of the DG and this distribution of labeled GCs was not different in mice exposed to a single episode of running (Figure S1D). Moreover, consistent with previous reports[19-21], we observed an asymmetry in neurogenesis, with a greater number of abDGCs in the SB compared to the IB (Figure S1G).

In order to determine the activation patterns of GCs (mGCs and abDGCs) when mice successfully performed a high cognitive demand spatial discrimination pattern separation task, TRAP2 mice were trained in a modified touch screen task that tests the ability to separate a unique pattern of illuminated squares posing a relatively low or high cognitive demand (Figure 1A and Figure S2A & B). The trial unique nonmatching-to-location (TUNL) task has been demonstrated to require the hippocampus, particularly when the cognitive demand is high when the separation of the sample to test squares is reduced, or the delay between sample and choice is increased[28,29]. Mice were injected with BrdU to birthdate neurons at day 0 (D0). At D7 mice were water restricted before EdU injections and shaping at D14 to habituate them to the operant task and learn to touch the screen for a saccharine water reward. Mice were then trained until they reached criterion (70% correct during one of two daily sessions on 2 consecutive days) in the TUNL task with a 1s delay between the sample and choice and a large (L) separation between sample panel and the test panel (Figure 1A and Figure S2A). Mice reached criterion on average at 10.7 ± 0.8 days in the large separation sessions (Figure 1B & D left panel). After reaching criterion the mice were tested with alternating trials of large and small (LS) separation between the sample and test panels. In this case the mice were always above criterion for the L trials but took another 9.3 ± 1.0 days to reach criterion on the S trials (Figure 1C & D middle and right panel).

Different cohorts of mice were analyzed at each level of cognitive demand of the task to assess the activation of mGCs and abDGCs. TRAP labeling was used to identify active neurons in the DG, together with thymidine analogs that birth-dated abDGCs at approximately 3 weeks (25 ± 1.4 days, EdU) and 5 weeks (39 ± 1.2 days, BrdU) of age (Figure 1E). We found a strong relationship between the level of cognitive demand of the task and the degree of mGC activation with a greater number of TRAP+ neurons in mice tested under higher cognitive load. Specifically, TRAP+ neuron density increased from shaping to the L separation stage, and was highest in mice performing the most cognitively demanding condition (LS) (Shap – LS, $p = 0.0007$; Shap – L, $p = 0.04$)(Figure 1F), regardless of whether the mice reach the criterion (C) or not (NC)(Figure S2H). A similar trend was observed when assessing c-Fos labeling 90 minutes after the final training session, further supporting the link between task demand and mGC activation (Figure S2F). Furthermore, when we examined the correlation between successful performance to criterion and the number of TRAP+ neurons, we found no significant relationship (Figure S2C), demonstrating that increased DG activity is driven by engagement in a high-demand task rather than task success.

However, when we examined the activation of two cohorts of abDGCs birth-dated with BrdU and EdU, we did not observe a relationship between the level of cognitive demand and the recruitment of newborn neurons. Only a small fraction (~1%) of 25- to 39-day-old abDGCs were active (TRAP+) during the high cognitive demand task (LS) (Figure 1G), regardless of whether the mice reached criterion (C) or not (NC) (Figure S2J). In contrast, mice that performed only the low-demand version of the task (L configuration) exhibited almost no TRAP-labeled birth-dated cells (Figure 1G). Moreover, in the shaping group, no newborn neurons were co-labeled with TRAP, indicating that minimal cognitive engagement does not recruit this population (Figure 1G).

In a separate cohort, we TRAPed neurons during the final day of LS trials and re-exposed mice to the same task 3 days later. After two LS sessions, mice were perfused 90 minutes later for immunohistochemical detection of endogenous c-Fos (Figure 1A). Task performance was reduced compared to the final day of prior training in both the L and S trials (Figure 1D, middle panel). Analysis of mGC reactivation (TRAP+/c-Fos+ cells) revealed greater overlap in mice performing LS trials than in those performing only L separations or shaping sessions (Shap–LS, $p = 0.05$; L–LS, $p = 0.01$) (Figure 1H). Notably, no $BrdU^+$ or EdU^+ cells were found to co-express TRAP and c-Fos, indicating that newborn neurons activated during the final LS session

were not reactivated three days later. Collectively, these results indicate that while increasing cognitive demand enhances activation and reactivation of mature granule cells, the recruitment of adult-born neurons remains low and does not scale with task difficulty.

Consistent with previous reports[10-13], we observed a bias in granule cell activity within the DG, with TRAP+ mGCs preferentially localized to the suprapyramidal blade (SB). Interestingly, this bias was not fixed but varied according to the level of cognitive demand of the task (Figure 2A). Mice performing the high-demand LS condition showed a pronounced enrichment of TRAP+ mGCs in the SB compared to the infrapyramidal blade (IB), driven by both an increase in labeled cells in the SB and a decrease in the IB ($p = 0.01$) (Figures 2A and S2E). In contrast, mice performing lower-demand versions of the task still exhibited a significant SB–IB difference, but the magnitude of this bias was reduced, resulting in a more balanced distribution of activity across blades. However, as with overall TRAP+ cell density, there was no significant correlation between individual task performance and the distribution of TRAP+ neurons in the SB (Figure S2D).

Further spatial mapping of TRAP+ cells relative to the hilus and dentate apex revealed that active neurons were concentrated in the outer radial portion of the granule cell layer—an area enriched in spatially tuned semilunar granule cells [11,30], and this localization was particularly evident after the high-demand LS task (Figures 2B and 2C). Together, these results demonstrate that the suprapyramidal bias in granule cell activity is dynamically modulated by cognitive demand, becoming more pronounced as task difficulty increases and producing distinct distributions of active neurons along both the apex–distal and hilar–outer axes of the DG (Figures 2D and 2E).

Activation of GCs during remote recall in the high cognitive demand task

We next investigated whether a similar spatially biased activity of GCs was observed in a remote recall (R) test three weeks after reaching the criterion during the initial training (I), and whether there was overlap in the population of active DG neurons (Figure 3A). In the remote session, mice had a high success rate performing close to criterion in the L trials on the first day of retesting suggesting that 3 weeks after initial learning they retained the ability in task (Figure 3B). However, when confronted with the more demanding trials with inclusion of the small separation configuration, mice required additional days to achieve the criterion level (Figure 3C), although most mice required less time to reach criterion in LS training during the remote trials than on the initial testing (Figure 3D). We again observed that the density of TRAP+ cells was

increased in mice that underwent LS compared to L only trials during the initial training (not shown) and importantly the distribution of active neurons during both the initial training (TRAP+) and remote training (c-Fos+) were biased to the SB after LS training (Figure 3F & G).

An analysis of birth-dated active neurons labeled during the initial training (TRAP+) or during the remote trials (c-Fos+) demonstrated a small number of BrdU (~4 weeks) neurons were labeled during the initial training (Figure 3H) whereas in the remote training we observed both BrdU labeled (7.7 weeks) and EdU labeled (5.7 weeks) abDGCs that were c-Fos+ only in mice after LS training (Figure 3I). No birth-dated abDGCs were found that were double labeled TRAP+ and c- Fos+, however we observed dual labeled mGCs with more TRAP+/c-Fos+ labeled neurons in mice that had performed LS training than those that only performed L training (p=0.0433) (Figure 3J).

Taken together, these results demonstrate that during initial training and remote training in the pattern separation task, spatially biased activity of neurons is observed in the SB but there is little overlap in activity of neurons in the DG of mice during these epochs of training.

mGC activity is required for DG function and efficient pattern separation in TUNL

Given that the suprapyramidal bias in DG activity scaled with cognitive demand, we hypothesized that altering the excitatory drive within the DG might modulate this spatial pattern of activation. We began by targeting mature granule cells (mGCs), the principal excitatory population in the DG, which are under strong inhibitory control and sparsely active in vivo[31,32].

To selectively suppress their activity, Dock10-Cre mice[33] were crossed with R26-LSL-Gi-DREADD mice (designer receptor exclusively activated by designer drugs) to express the inhibitory DREADD hM4Di, which can be activated by the ligand deschloroclozapine (DCZ)(50 $\mu g.kg^{-1}$)[34] during the LS sessions of the task (Figure 4C). Characterization of Dock10-Cre expression in newborn neurons (BrdU+) revealed few labeled cells at 2 weeks postmitosis, with progressively more double-labeled abDGCs in older, non-DCX–positive neurons (Figures 4A and S3), reaching ~80% of abDGCs by 7 weeks (Figures 4A and 4B). This pattern confirms that Dock10-Cre is expressed primarily in mGCs and older abDGCs. As predicted, DREADD-mediated inhibition of mGCs impaired task performance, with the majority of mice failing to reach criterion (62.5%) within the 14-day LS cutoff, compared to controls (34.8%) (p = 0.0452) (Figures 4D and 4E). Performance in the interleaved low-demand L trials was not affected (not shown). Consistent with reduced DG activity, we observed lower c-Fos expression in both the DG (p = 0.04) and CA3 (p = 0.006) of mice that did not reach criterion after 14 days (Figures 4F,

4G, and 4I). Interestingly, despite the overall reduction in activity, the distribution of active c-Fos+ neurons remained biased toward the SB, similar to control mice that reached criterion. This suggests that the overall excitability is a key feature of DG function during performance of a high cognitive demand pattern separation task (Figures 4H, 4J, and 4K).

DREADD inhibition of abDGCs disrupts blade-biased activity of mGCs and performance of mice in a high cognitive demand task

Having established that mGCs regulate overall DG activity but do not determine the SB-IB bias, we next asked whether manipulating abDGCs could influence this bias and the pattern of DG activation. Because mGC inhibition reduced global excitability without altering the spatial organization of active cells, this suggested that the blade-biased pattern may be set upstream by a more selective cell population. Given that abDGCs constitute a smaller, more plastic excitatory population, we hypothesized that selectively altering their activity might differentially affect both overall excitability and the spatial distribution of active neurons during high cognitive demand tasks. abDGCs are known to affect the excitability of mGCs[35,36] and there is a demonstrated blade bias in neurogenesis in the DG. However, it remains unknown whether abDGCs affect the blade-biased activity patterns of mGCs that are evident during a pattern separation task. To acutely modulate the activity of abDGCs during task performance, we created mice in which the inhibitory DREADD (designer receptor exclusively activated by designer drugs) could be conditionally expressed in abDGCs by crossing R26-LSL-Gi-DREADD mice (hM4Di)[37] to Ascl1^{CreERT2} mice. This selectively expresses the hM4Di inhibitory DREADD in a birth-dated cohort of abDGCs by the delivery of TAM (tamoxifen, see Methods) in the diet of mice for 7 weeks allowing the inhibition of their activity with a selective ligand deschloroclozapine (DCZ)(50 $\mu g.kg^{-1}$)[34] during the LS sessions of the task (Figure 5A & B) [38,39]. Inhibition of abDGCs (≤ 7 weeks old) using the DREADD ligand DCZ increased the time animals took to reach criterion compared to control groups of animals that received DMSO or were Cre negative (Cre-) ($p = 0.01$ and $p = 0.05$) (Figure 5C & D). This impairment was specific to the cognitively more demanding LS task, as inhibiting ≤ 7-week-old abDGCs did not affect the performance of mice once they had learned the L configuration (not shown). Importantly control groups that had also received TAM in their diet showed no effect in the pattern separation task or in the biased blade activity of mGCs (Figure 5C-J). Taken together this experiment suggests that abDGCs in this cohort (≤ 7 weeks) are beneficial to performance in a pattern separation task.

Prior work has demonstrated that abDGC loss causes an increase in activity of mGCs[35,40] which is likely through a loss of connections to hilar interneurons which provide feedback inhibition to the DG. Consistent with this, analysis of c-Fos in the DG demonstrated increased labeling across the DG when abDGCs were inhibited with DCZ activation of hM4Di compared to control groups ($p=0.0271$) (Figure 5E & F). Conversely, c-Fos+ labeling in the downstream CA3 region of the hippocampus demonstrated no significant difference in density between the control groups and abDGC inhibition (Figure 5G). Interestingly, we found that the biased distribution of c-Fos+ neurons in the two control groups showed the same profile as we had observed before in the IB and SB after mice perform the high cognitive demand task (Figure 5H). However, in the cohort of mice in which abDGCs were inhibited, the prominent biased distribution pattern of activity was not observed ($p = 0.01$) (Figure 5H). Furthermore, the distribution of c-Fos+ cells within the blades showed that when abDGCs were inhibited during LS training there was a marked prominence of labeled neurons located near the hilus in both the IB and SB in the region closest to the subgranular zone (SGZ), the neurogenic niche of the DG where abDGCs are produced, raising the possibility that these neurons are under greater feedforward inhibitory control via abDGCs (Figure 5I). In summary, DREADD inhibition of $\leq$ 7-week-old abDGCs during the LS high cognitive demand task resulted in a reduction in both in biased SB-IB spatial activity pattern as well as the activity labeling of neurons along both axes of the transverse DG (Figure 5J), and this altered activity correlated with a reduction in performance of animals which required increased days to complete the high cognitive demand task.

In the previous experiments we had provided TAM to mice in their diet to cause expression of hM4Di in neurons that range from 0 days to 7 weeks. This covers abDGCs that are within their critical period when they demonstrate strong plasticity and excitability and are well connected to the hippocampal network[41,42]. Because inhibition of this 0–7-week population altered both performance and the blade-biased spatial distribution of mGC activity, we next asked whether these effects depend specifically on the maturity of the abDGCs. To test whether younger, ≤4-week-old neurons contribute similarly to DG function during high cognitive demand, we provided TAM for only 4 weeks to restrict hM4Di expression to these younger abDGCs (Figure 6A). In the LS high cognitive demand task, there was no difference in the time to criterion of animals that had received DCZ administration for hM4Di inhibition of abDGCs compared to the control groups (Figure 6B). Similarly, analysis of c-Fos+ density in the DG found no difference in overall density (Figure 6C) and the blade distribution of active mGCs after hM4Di (Figure 6D) or in the hilar to molecular layer axes distribution (Figure 6E).

Taken together these results demonstrate that ≤ 7-week-old cohort of abDGCs that include neurons in their critical period of development influence the excitability and spatially biased pattern of activity of mGCs in the DG and also affect the performance of mice in a high cognitive demand pattern separation task. In contrast young neurons at ≤ 4 weeks do not influence either the performance of mice in the task or the spatial distribution of activity in the DG.

Discussion:

Blade-specific activation patterns in the dorsal dentate gyrus during high-demand discrimination

In this study we used activity labeling techniques combined with a complex, automated visual spatial pattern separation task to capture patterns of activity of GCs in the dorsal DG. The DG is a critical part of the hippocampal formation that receives extrinsic input from cortex and other structures but is also highly regulated by local connections with hilar and CA3 neurons[8]. While many roles have been ascribed to the dorsal DG, a prominent theory has been that its activity is vital to pattern separation[43]. We found that activity labeling of neurons demonstrated unique spatial distributions of active GCs which were amplified when the separation task was made more stringent for the mice. In particular, we observed a biased distribution of active neurons in the SB, which was elevated in mice that completed the LS task. There have been prior descriptions of a blade-biased distribution of active neurons when mice engage in hippocampal dependent behaviors[10-13] however it is still not known how these spatially defined activity patterns are modulated or established. We found that not only is there a bias towards more activity in SB and less in the IB during a more demanding task, there is also an increase in activity density in the outer radial areas of the granule cell layer (GCL) where semilunar granule cells are enriched[11,30], and in regions closer to the dentate apex. These elevated biased spatial distributions of active neurons were not observed when mice were assessed after running or after the low cognitive demand version of the task, two behaviors that increase the activity of mGCs significantly but do not enhance their blade-biased distribution (Figure S2E). However, while blade-specific differences in activity are evident, no distinct, independent microcircuit has been identified that exclusively governs the function of either the SB or IB. This raises an important question as to whether these differences arise solely from variations in afferent connectivity and intrinsic GC properties or if they reflect an underlying, segregated network organization within the DG. Future studies exploring whether the SB and IB operate as distinct computational units or as interconnected components of a larger network will be essential to clarify the functional basis of this observed bias.

Activity level of mGCs is required for a high demand task

Mature granule cells (mGCs) constitute the primary excitatory population of the DG and are essential for its sparse coding properties. Despite their large number, mGCs are strongly regulated by local inhibition and typically remain sparsely active in vivo[31,32]. In our study, we used an acute and reversible DREADD inhibition of mGCs using a Cre driver line expressed in mature but not in young adult-born neurons (Figure 4A, S3). Suppressing mGC activity during the LS task had a major effect on performance: most mice in the inhibited cohort failed to reach criterion. Analysis of behavior revealed that during S trials, performance remained at chance, whereas in interleaved L trials, mice continued to perform above criterion. Consistent with reduced mGC excitability, the density of c-Fos+ neurons was significantly decreased in the DG. Interestingly, despite this reduction in overall activation, the blade-biased distribution of active neurons was still evident in mice that performed the task but failed to reach criterion. Thus, unlike the effects observed when inhibiting adult-born neurons, there was no clear correlation between behavioral impairment and changes in the spatial distribution of active cells. Direct inhibition of mGCs therefore produced a fundamentally different outcome on DG circuit dynamics and task performance. While abDGC inhibition slowed performance and altered the spatial distribution of active mGCs even in mice that reached criterion, direct suppression of mGCs reduced global excitability without changing the spatial organization of active cells in animals that did or did not reach criterion (not shown). Moreover, the subset of mice that did reach criterion performed with latencies indistinguishable from control cohorts.

Prior studies using genetic manipulations to increase neurogenesis, have identified blade-specific changes in the number of c-Fos+ cells, with an increase in the IB following contextual discrimination[44], and a corresponding increase or decrease in the IB or SB respectively, after navigational learning[45]. These prior findings support the hypothesis that the SB is context-specific and involved in pattern separation, while the IB is more associated with spatial representation and memory precision[46]. Our study extends these observations by demonstrating that while overall mGC excitability is required for successful performance in high cognitive demand conditions, the SB–IB bias itself can persist independently of excitatory drive, suggesting that it is not directly determined by mGC activity.

Adult-born granule cells modulate DG network organization during high cognitive demand

The DG, uniquely among temporal lobe structures, contains a neurogenic niche where new neurons are continuously generated and integrated into the existing network. Post-mitotic adult-born dentate granule cells (abDGCs) mature over several weeks[47], reaching maturity by around 8 weeks post mitosis where their functional properties and connectivity resemble those of other

mGCs[48,49]. During a critical period between 4–8 weeks, however, they exhibit heightened plasticity and distinct circuit interactions[50], making them uniquely positioned to influence local computation.

It has been proposed that abDGCs modulate local circuit activity by contributing to the sparsity of mGC firing through feedback inhibition[50-52] or through direct inhibition[53]. This inhibitory influence is largely mediated by diverse interneuron populations in the DG, including parvalbumin-positive (PV+), somatostatin-positive (SOM+), and neuropeptide Y-positive (NPY+) interneurons, which play crucial roles in regulating the excitability of GCs. Given their importance in enforcing sparse coding, these interneurons could be key modulators of the SB-IB activity differences observed in our study, yet their precise contribution to blade-specific activation remains unclear.

Consistent with prior behavioral work implicating the DG in pattern separation[54], manipulations that ablate abDGCs impair discrimination when task difficulty increases[55] , whereas genetic or environmental manipulations that enhance neurogenesis improve discrimination performance[56,57]. In our study, only limited numbers of abDGCs were labeled during task performance, as expected given their low population size relative to mGCs. However, neurons that were approximately seven weeks post-mitosis were more prominently labeled than those four weeks post-mitosis, consistent with the notion that older abDGCs are more integrated into the local circuit. Despite their small number, these neurons exerted a disproportionate influence on DG activity.

Using an acute, reversible chemogenetic inhibition of different abDGC cohorts during task performance[39] , we observed that suppression of ≤7-week-old abDGCs increased mGC activity, consistent with prior studies that chronically reduced neurogenesis[35]. More importantly, inhibition of abDGCs during the LS task impaired performance in high-demand discrimination trials without affecting already-learned, low-demand trials within the same session. This manipulation disrupted the normal SB-biased pattern of mGC activation seen in controls, as well as the typical distribution of labeled mGCs along the hilar–molecular layer and apex–tip axes of the DG. These effects were specific to the inhibition of ≤7-week-old abDGCs and were not observed when younger (≤4-week-old) or older abDGC populations were targeted. These findings suggest that abDGCs exert their influence not through direct encoding, but through regulating inhibitory tone within the DG microcircuit, potentially via PV- or SOM-positive interneurons that shape granule cell recruitment.

Together, these results reveal complementary but distinct contributions of mGCs and abDGCs to DG function. mGCs provide the essential excitatory output required for encoding and task

performance under high cognitive demand, whereas abDGCs modulate this activity to establish the structured, blade-biased distribution of mGC activation necessary for optimal discrimination. This modulation likely arises through transient inhibitory control during the critical period of abDGC maturation, allowing the DG to dynamically tune its excitability and spatial coding to match task difficulty. Our findings support a model in which efficient pattern separation relies on both the stable excitatory scaffold provided by mGCs and the adaptive, modulatory influence of maturing abDGCs on DG network organization. This aligns with and extends prior models by showing that it is the maturing cohort, not immature or fully mature abDGCs—that provides this modulatory control.

Limitations of the Study

The use of activity tagging has the inherent limitation that it provides a snapshot in time of activity during a window and more nuanced effects of activity patterns during the behaviors are not captured. This is countered by the less invasive nature of these experiments than ones that require implants for in vivo recording of neuron activity, which are themselves not fit for purpose because they cannot capture the spatial distribution in the subregions of the DG effectively. Future studies using *in vivo* measurements of activity will be required to support the present findings and find conclusive neural representations required for discrimination of similar patterns. A second limitation is that the mechanisms of the blade biased activity are yet to be discovered. Future work will be needed to assess this to further elucidate the importance of these patterns of activity to computations in the DG.

Materials and methods

Ethics statement: All animal procedures were conducted in accordance with protocols approved by the Northwestern University Institutional Animal Care and Use Committee (IACUC). Male and female mice were housed 3–5 per cage on a reverse light/dark cycle of 12/12 hours within a controlled environment. They received food and water *ad libitum*. All behavioral testing was conducted during the animals' dark cycle and was conducted by experimenters blinded to genotype. Tail biopsies were collected for genotyping via PCR. All efforts were made to minimize the number of mice used and to reduce any potential pain or stress, in line with ethical guideline.

Animals: All mouse lines were maintained on a C57Bl/6 background. Mice were propagated by female breeders heterozygous for Cre recombinase and homozygous for either the Ai9 allele (Rosa-CAG-LSL-tdTomato-WPRE) or hM4Di allele (R26-LSL-Gi-DREADD) with male breeders homozygous for Ai9 or hM4Di. TRAP2;Ai9 mice were generated by crossing Fos^{2A-}

$^{iCreER/+}$ (TRAP2) mice (Jax #030323)[23] with Ai9 (Jax #007909) mice to generate double-heterozygous mice. Ascl1-CreER^{T2};hM4Di mice were generated by crossing R26-LSL-Gi-DREADD mice (Jax #026219) [37] with mice carrying tamoxifen-inducible Cre recombinase under the control of the *Ascl1* promoter (Jax #:012882) [58] to generate double-transgenic progeny Ascl1-CreER^{T2};R26$^{LSL-hM4Di}$. Cre-negative littermates from heterozygote breedings were used as controls. Dock10-Cre;hM4Di mice were generated by crossing Dock10-Cre [33] mice with hM4Di mice to produce double-transgenic progeny Dock10-Cre;R26$^{LSL-hM4Di}$.

Birth-dating of abDGCs: 6–8-week-old mice received three intraperitoneal (i.p.) injections of 5-Bromo-2′-deoxyuridine (BrdU, Sigma Aldrich #B9285) at 100 mg/kg (i.p) at 4 hours intervals on a single day [59]. Two weeks later, 5-Ethynyl-2′-deoxyuridine (EdU, Sigma Aldrich, #900584) was administrated following the same injection protocol.

Tamoxifen administration: *IP injections:* To time the labeling of TRAP+ cell in TRAP2 mice, 4-hydroxytamoxifen (4-OHT; Sigma Aldrich, #H7904) was administered intraperitoneally. 4-OHT was dissolved at 20 mg/mL in pure ethanol and stored at –20°C for up to several weeks. Before use, 4-OHT was redissolved in corn oil (Sigma, Cat #C8267) and heated to 90°C with shaking until the ethanol had evaporated yielding a final concentration of 10 mg/mL. The final 10 mg/mL 4-OHT solutions was used on the day it was prepared. All injections were delivered intraperitoneally at 50 mg/kg either at the end of the training phase of the day or 2 hours after running.
Oral administration: For conditional expression of hM4Di in *Ascl1-CreER^{T2}* cells, a tamoxifen diet (TD.130858, Envigo) was provided *ad libitum* for 4 or 7 weeks, depending on the experimental timeline. Body weight was carefully monitored daily. The chow contained 500 mg tamoxifen/kg, delivering ~80 mg tamoxifen/kg body weight per day, assuming an average mouse weight of 20-25 g and a daily intake of 3-4 g.
Mice were monitored daily for signs of stress, discomfort, or adverse effects related to tamoxifen exposure.

Inhibitory DREADD-hM4Di activation: Deschloroclozapine (DCZ, MedChemExpress #HY-42110) was dissolved in 2% DMSO in 0.9% saline and administered by i.p. injections at a dose of 50 µg.kg^{-1} [34]. Behavioral trials started 30 minutes after drug administration.

Behavioral procedures: Adult (8-10 weeks-old) male and female mice were used in behavioral studies. To acclimate the mice to handling before behavioral testing, all animals were handled by the experimenter for 2 min per day for 3 consecutive days.

Running wheels: To habituate the mice to running, wireless running wheels (ENV-047, Med Associates) were placed in their home cage for 5 days (maximum 5 mice per cage). Two days prior to BrdU injections, the wheels were removed from the cage. One week before the experiment, mice were individually housed. On the day of the experiment, a running wheel was added to each cage for a duration of 4 hours. After 2 hours, mice received a 4-OHT injection and were returned to their respective cages. Following an additional 2 hours of running, the wheels were removed from the cages. Three days later, wheels were reintroduced to the cage and remained until mice were euthanized for assessment of TRAP+ cells, 90 minutes after the beginning of the run. The effect of exposure to the wheels was quantified by measuring the total distance run by each mouse.

Automated touch screen operant behaviors: Testing was conducted in custom-built, touch screen-based automated operant device boxes designed specifically for mice, the Operant House (doi.org/10.1101/2025.01.24.634815). The apparatus consisted of a rectangular modular testing chamber (w14.5cm x l21.5cm x h18.5cm). A 60mW green LED was located above a port that gave access to a retractable water bottle at the back of the chamber. At the opposite end of the chamber, a flat-screen infrared touch monitor was controlled by custom scripts (Python). In front of the touchscreen was a mask with 2 horizontal lines of 5 squares. Mice performed a modified version of the “trial unique nonmatching-to-location” (TUNL) task [29]. Five days prior to testing and during the training phase, mice were placed on a water-restriction regime, with access to water for 10 minutes per day, and were maintained at 85-90% body weight during the entire duration of the experiment. Mice were trained each day, in two separate sessions of 30 trials or a maximum of 30 minutes. Experiments began with “Shaping” in which, following habituation to the operant chamber for 30 minutes, mice were trained to touch a lit white square stimulus presented randomly in one of the response windows of the touch screen in order to receive a reward (2 seconds water nozzle access with saccharin water 0.01%). Mice were trained in Shaping until they successfully achieved 30 rewards within 30 min during 3 successive sessions. Mice were then transitioned to training in the TUNL task with a Large-only separation (L configuration). For this task, each trial was composed of two phases. During the sample phase, a white square was illuminated in one of the 10 possible locations on the screen (Figure S2A & B). Following a nose-poke to the sample square the stimulus disappeared, and the mouse received a reward only on 33% of the trials. After a 1s delay from the sample trial, the choice trial was initiated where two stimuli were presented one in the repeated sample location (incorrect) and the other in the new location (correct) separated spatially by 4 squares in the L configuration (Figure S2A & B). A touch to the correct sample location resulted in a

reward and an 5s inter-trial interval (ITI) before the next trial was initiated. An incorrect choice resulted in a 10 second punishment (roof lights ON) and then an ITI, followed by correction trials during the first two days of training. Correction trials followed the same procedures, except that the same sample and choice locations from the previous incorrect trial were presented again until the correct choice was made. The correction trials were not included in performance calculations. After successfully completing 30 trials within 30 minutes at over 70 % correct for at least two out of four sessions on two consecutive days in the Large configuration, the mice were transitioned to the next phase of the TUNL task with combined sessions with presentation of stimuli with both Large separation and Small separation between sample and choice squares (LS configuration). Training followed the same pattern as previously described except that there were two separate possibilities for the presentation of the choice square which was either separated by 4 squares from the sample square during L trials, or the choice square was 0-1 square separated from the sample location during S trials (Figure S2B). Mice trained in the LS phase with 15 of each alternating L and S trials, until they reached criterion which was set at 70 % successful S configuration trials in two out of four sessions on two days. A proportion of mice did not reach the criterion in LS within the allotted time across all experimental groups (~25%-30%, Figures S2G).

Immunohistochemistry: Mice were deeply anesthetized with isoflurane and then perfused transcardiacly with PBS containing 0.02% sodium nitrite followed by 2% paraformaldehyde (PFA) in 0.1 M sodium acetate buffer (pH 6.5) for 3 min, and 2% PFA in 0.1 M sodium borate buffer (pH 8.5) for 10 min [60]. Brains were dissected and post-fixed in 2% PFA 0.1 M sodium borate buffer (pH 8.5), for 24-48 hours and stored at 4°C in PBS until sectioning. 50µm floating sections were collected on a Leica Vibratome VT1000 and stored at 4°C in PBS containing 0.02% sodium azide. For c-Fos analysis, perfusions were performed 90 minutes after the end of the behavioral training. Immunohistochemistry was conducted at room temperature using standard procedures. Free-floating sections were incubated for 30 min in a solution of 25 mM glycine to decrease the background signal and then rinsed two times in Tris-Buffered Saline 1X (TBS). Sections were then blocked for 1 hour in the saturation solution containing TBS-Triton (0.25% Triton X-100 (Fisher, BP151-100), 3% normal donkey serum (NDS; Jackson ImmunoResearch, 017-000-121) and 0.1% bovine serum albumin (BSA; Sigma, A9085)). The sections were then incubated overnight in the saturation solution containing the primary antibody (rabbit anti c-Fos (1/1500, Cell Signaling), sheep anti-BrdU (1/2500, NovusBio), rabbit anti RFP (1/5000, Abcam)). For c-Fos staining, no serum and BSA were used. For BrdU staining, sections were incubated for 10 mins in a solution of DNAse I (Sigma #D5025, 15

KU/mL dissolved in 0.05 M NaCl), $MgCl^2$ (6 mM) and $CaCl^2$ (10 mM) to cleave DNA then rinsed 2 x 5 min in TBS before the saturation part. For EdU staining, sections were incubated in solution from the kit ClickIT™ (#C10340 Thermofisher) during 30 min then rinsed 2 x 5 min TBS before the saturation part. No antibodies were necessary for the rest of the immunostaining. The next day, sections were washed 2x5 min in TBS before being incubated for 1 hour in secondary antibody solution (donkey anti-rabbit Alexa 647 or 488 (1/1000, Invitrogen), donkey anti-sheep Alexa 488 (1/1000, Invitrogen)). Finally, sections were washed 2x5 min in TBS and cover-slipped with ProLong Diamond mounting media 275 containing DAPI (#P36962, ThermoFisher Scientific).

Imaging and neuron quantification: Analyses were conducted in the dorsal DG, as prior studies have demonstrated its involvement in spatial memory and the fine-grained contextual differentiation required for pattern separation. The dorsal hippocampus is crucial for encoding and distinguishing spatial information, which is central to this process. In contrast, the ventral DG is more strongly associated with emotional processing and affective memory rather than high-resolution spatial encoding needed for pattern separation.

Confocal images were obtained with a Zeiss microscope (LSM700) with a 20x objective with the experimenter blind to the genotype and condition following previous protocols [59]. One section in every ten serial sections were analyzed through the dorsal hippocampus (stereotaxic coordinates: -1.20 to -2.30 relative to bregma according to Paxinos' brain atlas). Two to three 10 µm z-stack acquisitions, were made to picture the whole dentate gyrus in each section. 3D reconstructions were used to univocally verify co-localization (e.g. activated mature neurons or immature neurons). All acquisitions were carried out in sequential scanning mode to prevent cross-bleeding between channels. Stacks of images were then reconstituted using Fiji software, allowing the experimenter to count the number of cells. The surface area of the dorsal hippocampus, DG, SB, IB and CA3 were traced in mapping software (Neurolucida Zeiss) using a 10x objective. The volume was determined by multiplying the surface area by the distance between sections (500 µm). Densities of BrdU+, EdU+, TRAP+ and c-Fos+ cells were estimated by multiplying the total number of labeled cells by 10. For immunohistochemical analysis, a subset of approximately 5 mice from the behavioral cohorts of ~15 mice were randomly selected. If the results exhibited high variability, one or two additional mice were included to improve data precision. Selection remained random throughout. This approach was chosen to balance the workload associated with immunohistochemistry while ensuring sufficient statistical

power; given that behavioral experiments require larger sample sizes to achieve robust significance only a subset could be included in this analysis.

Distribution of TRAP+ and c-Fos+ Cells in the DG: We followed methods presented in literature [61]. Using stacks of images obtained from confocal microscopy, the localization of TRAP+ and c-Fos+ cells in the DG was assessed using Fiji software. *Distance from the hilus:* The contours of each blade were manually outlined and the distance from the center of each cell body to the hilus was manually measured. Cells located in the apex region were excluded from the counting.

Distance from the apex: Excluding the apex region, the size of each suprapyramidal blade was measured as well as the distance of each cell from the apex. These distances were then expressed as percentage of total blade length.

Statistical analysis: Data are expressed as means ± SEM. Statistical analysis was performed using Statview and Origin programs. For behavioral experiments, one sample *t*-tests were used to compare performance against chance (50% in the TUNL experiment). For histochemical data, we used independent comparisons with Mann–Whitney U test for non-paired samples (non-parametric). To test more than two independent samples we used the Kruskal Wallis test. In case of significance, a post hoc pairwise comparison (Dunn's test) was made to identify the group that differed. Differences were considered to be significant when $p < 0.05$.

Figure Legends:

Figure 1 : **TRAP labeling of mGCs and birth-dated abDGCs after the TUNL pattern separation task**

(A) *Top:* Schematic illustrating the pattern separation paradigm. Male (n = 9) and female (n = 7) mice (6-8-week-old) received 3 injections of BrdU at D0 and 3 injections of EdU two weeks later (D14) before starting the behavioral paradigm. Mice received one injection of 4-OHT on the day they reached criterion (TRAP) and were perfused 3 days later 90 minutes after one exposure to the behavioral paradigm to allow endogenous c-Fos expression (c-Fos). Control mice (males n = 6, females n = 4) underwent the same treatment but only participated in the Large separation task (L). Mice were water-restricted during the behavioral experiment. *Bottom:* Cartoon representation of the chamber in TUNL task with examples of Large separation (L) and Small (S) separation configurations. High cognitive demand paradigm consisted of interleaved L and S trials (LS).

(B) Number of days for each mouse to reach the 70% success criterion in the Large separation (L).
(C) Number of days for mice to reach 70% success criterion in S trials, during the LS separation task.
(D) *Left*: Average percentage of correct choices (% success) in the L separation on the first day of training, as well as during the three days prior to reaching criterion (days before criterion, DBC) and the day of reaching the criterion (crit)(one-sample *t*-test to chance at criterion Large $t(16)=12.04$, $p<0.0001$). *Middle*: Average percentage of correct choices in the L and S separation on the first day of training, during the three days before criterion (DBC), on the day of reaching criterion and 3 days later (one-sample *t*-test to chance at criterion Large $t(16)=8.38$, $p<0.0001$; Small $t(16)=7.37$, $p<0.0001$). *Right:* Cumulative probability of days to criterion of mice in S for both controls L and LS groups.
(E) Example section of BrdU+ labeling (green) EdU+ labeling (blue) and TRAP+ labeling (red) in TRAP2 mice. Calibration bar: 30 µm.
(F) Density of TRAP-labeled GCs in mice undergoing LS compared to control mice engaged in either shaping (Shap) or the Large configuration task only (L) ($H(2) = 12.2$, $p =0.002$; Kruskal Wallis)(With Dunn post hoc analysis: Shap comparison to L, $p = 0.25$, Shap comparison to LS, $p=0.0007$, L comparison to LS $p = 0.04$).
(G) Percentage of BrdU labeled cells (39 days +/- 1.23) or Edu labeled cells (25 days +/- 1.37 days) also TRAP+ after L or LS training (BrdU+/TRAP+ L: 0.145 ± 0.145 %, 6 mice; LS BrdU+/TRAP+ 0.822 ± 0.474 %, 6 mice; ns; EdU+/TRAP+ L: 0.203 ± 0.144 %, 6 mice; LS BrdU+/TRAP+ 0.304 ± 0.155 %, 7 mice; ns; Mann–Whitney).
(H) Percentage of TRAP+ GCs expressing c-Fos+ in Shap, L or LS task after reaching criterion (expressed as a percentage of TRAP+ cells) ($H(2) = 7.7$, $p =0.02$; Kruskal Wallis)(With Dunn post hoc analysis: Shap comparison to L, $p = 0.64$, Shap comparison to LS, $p=0.05$, L comparison to LS $p = 0.01$).

Figure 2: **Blade-biased activity of mGCs during a high cognitive demand pattern separation task**
(A) Spatial distribution of TRAP-labeled cells in the infrapyramidal (IB) and suprapyramidal (SB) blades of the dorsal DG in TRAP2 mice performing the LS separation, compared to control mice that performed only the L configuration. TRAP+ neurons showed a preferential distribution to the SB over the IB in the DG, with a more pronounced bias in the LS group of mice ($H(2) = 8.54$, $p =$

0.01; Kruskal Wallis)(With Dunn post hoc analysis: Shap comparison to L, p = ns, Shap comparison to LS, p=0.02, L comparison to LS p = 0.01).
(B) Spatial distribution of TRAP+ cells in the hilar to outer radial GCL axes in the SB (0 to 120µm) and the IB (0 to 120µm) of the dorsal DG with 0 µm indicating location at the hilar border.
(C) Distribution of TRAP-labeled cells along the apex to blade extremity axes of the SB of the dorsal DG, with 0% indicating location at the dentate apex (Shap: 0-50: 30.2 ± 4.4%, 4 mice, 50-100: 68.3 ± 4.4%, 4 mice; p= 0.02; L: 0-50: 51.9 ± 2.18%, 6 mice; 50-100: 48.1 ± 2.18%, 6 mice; ns ; LS : 0-50: 56.0 ± 2.44%, 6 mice; 50-100: 43.8 ± 2.54%, 6 mice; p= 0.0065; Mann–Whitney).
(D) Example section of TRAP+ cells in the dorsal DG illustrating the distinct boundaries between the two blades, the hilus, and the apex. Calibration bar: 50 µm.
(E) Cartoon illustrating the two blades of the DG: IB and SB. Dentate granule cells are depicted in grey while red circles represent TRAP+ cells in the DG. In the L group, a greater number of labeled cells are localized in the SB compared to the IB. This bias of activity is also observed in the LS group, where the bias is more pronounced, and the overall activity of the DG is increased. In the SB, the majority of the activated cells are located closer to the tip of the blade.

Figure 3: **Activation of GCs during remote recall in the high cognitive demand task**
(A) Schematic representation of the pattern separation paradigm used in the study. Mice (male n=11, female n=8) performed two trainings sessions: initial (I) and remote (R). The second training (R) took place 3 weeks after the mice reached the S criterion in LS. Mice were perfused when they reached the criterion in S during R. A second group that performed only in the L configuration during both training sessions was included as control (males n=3, females n=3).
(B) Learning curves representing the percentage of success during the remote test (R) for the L (green) and LS (orange) groups (one-sample *t*-test to chance at criterion; LS: Large t(14) = 11.8, p < 0.0001, Small t(14) = 10.3, p<0.0001; L: Large t(3) = 6.78, p = 0.0066).
(C) Percentage of mice reaching the L and S criterion in LS group, during the remote test (R) represented as cumulative probability. During the remote test, mice reach the L criterion in just a few days but require more time to reach the S criterion.
(D) Performance of individual mice indicating a non-significant reduction in the number of days needed to reach the criterion between the initial and remote training sessions. Only 4 mice (red lines) required more days to reach the criterion during the remote test. (I: 8.067 ± 1.173 %, R: 5.93 ± 0.753, 15 mice; p= 0.204; Mann–Whitney).

(E) EdU labeled cell that was also TRAP+ labeled after the initial training but was that was not reactivated (c-Fos) during the remote test. EdU (green), TRAP (red), c-Fos (blue) in TRAP2 mice. Calibration bar, 10 µm.
(F) Distribution of TRAP-labeled cells in the IB and SB blades of the dorsal DG in TRAP2 mice. Labeling was performed in LS separation during initial training (I) and compared to control mice that performed only the L configuration. Active neurons show a preferential distribution to the SB over the IB in the DG. This bias is more prominent in the LS group of mice (training I: IB : L: 47.3 ± 3.312 %, 4 mice; LS : 33.7 ± 3.31 %, 4 mice; p = 0.021; SB : L: 52.7 ± 3.32 %, 4 mice; LS : 66.4 ± 3.31 %, 4 mice; p= 0.021; Mann–Whitney).
(G) Distribution of c-Fos labeled cells between the IB and SB blades of the dorsal DG in TRAP2 mice performing the LS separation during remote training (R), compared to control mice that performed only the L configuration. Active neurons show a preferential distribution to the SB over the IB in the DG (LS, IB : 31.4 ± 3.11 %, 4 mice; SB : 68.7 ± 3.11 %; p=0.021; Mann–Whitney). The bias of activity is similar between the two groups (R, IB : L: 41.1 ± 4.18 %, 4 mice; LS : 31.4 ± 3.101 %, 4 mice; p= 0.191; SB : L: 58.9 ± 4.18 %, 4 mice; LS : 68.7 ± 3.11 %, 4 mice; p= 0.191; Mann–Whitney).
(H) Percentage of newborn neurons (BrdU (7.7 weeks) or EdU (5.7 weeks)) activated during the initial training (I), as indicated by co-labeling of $TRAP^+$(BrdU+ c-Fos+: L: 0.242 ± 0.242 %, 6 mice, LS: 0.170 ± 0.170 %, 6 mice; ns ; Mann–Whitney).
(I) Percentage of newborn neurons (BrdU or EdU) activated during the remote test (R), as indicated by c-Fos expression (BrdU+ c-Fos+: 0.977 ± 0.426 %, 6 mice, p=0.05; EdU+ c-Fos+: 0.694± 0.317 %, 9 mice; p= 0.0785; Mann–Whitney).
(J) Percentage of mGCs activated during the (I) training ($TRAP^+$) that were reactivated during the R test (c-Fos+) (expressed as a percentage of TRAP+ cells) (TRAP+ c-Fos+: I: 0.764 ± 0.309 %, 4 mice; R: 1.68 ± 0.067 %, 4 mice; p= 0.0433; Mann–Whitney).

Figure 4: **DREADD inhibition of mGCs during a high cognitive demand task**
(A) Percentage of BrdU-labeled cells that are also Dock10+ at different time points following BrdU injections (in days).
(B) Representative section showing BrdU+ labeling (green) and Dock10+ labeling (red) in Dock10 cre;Ai9 mice. Calibration bars: 10 µm.
(C) Schematic representation of the pattern separation paradigm. All mice (males n = 17, females n = 27) received DCZ i.p. injections 30 minutes before the beginning of their LS trials.

(D) Percentage of mice reaching criterion in (S) and percentage that were not successful (NS) after 14 days of training in S configuration of LS. A majority of mice never succeeded in reaching the criterion in the Cre+ DCZ group ($z = 2.00$, $p = 0.0453$, z-test - Group NS).
(E) Percentage of mice reaching the criterion in S trials across days represented as the cumulative probability including all successful and not successful mice in the group.
(F) Density of c-Fos+ GCs in the dorsal DG across the two groups. A significantly reduced density was observed in the Cre+ DCZ group compared to controls (DG, Cre+ DCZ: 8933.9 ± 556.4 mm^3, 6 mice; Cre- DCZ: 13578 ± 2135 mm^3, 5 mice; $p = 0.045$; Mann–Whitney).
(G) Density of c-Fos+ GCs in the dorsal CA3 across the two groups. A significant reduction was observed in the Cre+ DCZ group compared to the control groups (CA3 Cre+ DCZ: 20647 ± 1309 mm^3, 6 mice; Cre-DCZ: 34500 ± 2665 mm^3, 5 mice; $p= 0.0062$; Mann–Whitney).
(H) Blade specific distribution of c-Fos+ GCs in the IB and SB of the dorsal DG in mice performing LS separation (IB: Cre- DCZ: 31.5 ± 2.47 %, 5 mice; Cre+ DCZ: 27.2 ± 2.55 %, 6 mice; ns; SB: Cre- DCZ: 68.6 ± 2.47 %, 5 mice; Cre+ DCZ: 72.8 ± 2.55 %, 6 mice; ns; Mann–Whitney).
(I) Example of dorsal DG section from Dock10-cre:hM4Di mice after LS training. c-Fos+ neurons are labeled in red, DREAD-hM4Di (=Dock10+) neurons expressing citrine are labeled in green. Calibration bars: 100 µm.
(J) Spatial distribution of c-Fos+ along the hilar to outer radial GCL axis of the DG (0 to 120µm), with 0 µm indicating location at the hilus.
(K) Cartoon illustrating the distribution of activity labeled GCs in the SB and IB blades of the DG. GCs are depicted in grey while red circles represent activated cells in the DG. The overall distribution of neurons in mice in which mGCs were inhibited (Cre+ DCZ) and which did not reach criterion was not different to controls even though the total density of activity labeled neurons was lower.

Figure 5: **DREADD inhibition of ≤ 7-week abDGCs during a high cognitive demand task**
(A) Schematic representation of the pattern separation paradigm. Prior to onset of the training, mice (males n = 17, females n = 16) were provided tamoxifen-containing food ad libitum in the home cage for 7 weeks to activate TAM inducible Cre recombinase (Ascl1-CreER^{T2}) in abDGCs. All mice received DCZ (deschloroclozapine, 50 $\mu g.kg^{-1}$) or DMSO injections 30 minutes before the beginning of LS trials.

(B) Example section from Ascl1-CreER^{T2}; hM4Di mice after LS training. c-Fos+ neurons are labeled in red, TAM induced neurons expressing citrine are labeled green. Calibration bars *top*: 140 µm *bottom*: 50 µm.
(C) Percentage of mice reaching the criterion in the S trials across days represented as the cumulative probability. The Cre+ DCZ treated group needed additional days to reach criterion compared to controls.
(D) Number of days for each mouse to reach the 70% success criterion in S trials, (H(2) = 6.29, p=0.043; Kruskal Wallis)(Cre+ DCZ comparison to Cre+ DMSO, p = 0.017; Cre+ DCZ comparison to Cre- DCZ, p = 0.05 with Dunn's multiple comparison post hoc analysis).
(E) c-Fos+ cell density in all groups of mice. There was an increase in c-Fos+ mGCs in mice in which ≤ 7 week abDGCs were inhibited by DCZ (H(2) = 7.22, p=0.0271; Kruskal Wallis)(Cre+ DCZ comparison to Cre+ DMSO, p = 0.014; Cre+ DCZ comparison to Cre- DCZ, p = 0.027 with Dunn's multiple comparison post hoc analysis).
(F) Example section after c-Fos immunohistochemistry to assess distribution of c-Fos+ mGCs between the IB and SB of the dorsal DG in groups of mice who received DCZ (cre- vs cre+). c-Fos cells are localized closer to the hilus in the Cre+ group. Calibration bar, 100 µm.
(G) c-Fos+ density in the CA3 region of the hippocampus in each of the groups of mice. No significant difference was observed in any of the groups (H(2) = 3.9, p =0.142; Kruskal Wallis).
(H) Blade distribution of c-Fos+ mGCs in the IB and SB of the dorsal DG in mice performing the LS separation receiving either DCZ or DMSO 30 min prior to task performance. Active neurons are distributed preferentially to the SB than the IB in the DG for the control groups. However this distribution bias is significantly reduced in Cre+ DCZ group (IB: H(2) = 8.91, p = 0.012; SB: H(2) = 8.910, p = 0.012; Kruskal Wallis)(Cre+ DCZ comparison to Cre- DCZ p = 0.0032; Cre+ DCZ comparison to Cre+ DMSO p = 0.036 with Dunn's multiple comparison post hoc analysis).
(I) Spatial distribution of c-Fos+ GCs along hilar to molecular layer axes of the SB (0 to 120µm) and the IB (0 to 120µm) of the dorsal DG, with 0 µm indicating the hilar position. c-Fos+ cells are localized closer to the hilus in the Cre+ DCZ group.
(J) Cartoon illustrating the DG with its two blades: IB and SB. Dentate granule cells are depicted in grey while red circles represent activity labeled cells in the DG. For Cre+ DCZ mice, the distribution of labeled neurons is closer to hilus, away from outer radial GCL and more evenly distributed in IB and SB.

Figure 6: **DREADD inhibition of ≤ 4-week-old abDGCs does not affect performance of mice**

(A) Schematic representation of the pattern separation paradigm used in the study. Prior to the behavioral experiment, mice (males n = 12, females n = 23) were given tamoxifen-enriched food for 4 weeks to activate the Cre recombinase and label newborn neurons. All mice received DCZ or DMSO injections 30 minutes before the beginning of LS trials.
(B) Number of days for each mouse to reach the 70% success criterion in S trials (H(2) = 4.21, ns; Kruskal Wallis).
(C) Density of c-Fos+ GCs in the dorsal DG across the different groups (DG: H(2) = 0.404, ns, Kruskal Wallis)
(D) Blade specific distribution of c-Fos+ cells in the IB and SB of the dorsal DG in mice performing LS separation (H(2) = 0.46, ns ; Kruskal Wallis).
(E) Spatial distribution of c-Fos+ along the hilar to outer radial GCL axis of the DG (0 to 120µm), with 0 µm indicating location at the hilus.

Figure Sup 1: **Activity labeling of GCs after running**
(A) Schematic representation of the running paradigm. Prior to the behavioral experiment, mice (males n = 30, females n = 3) were injected with BrdU. After Δ weeks, the mice were allowed to run for 2 hours before receiving a 4-OHT injection, followed by an additional 2 hours of running. Mice were perfused 3 days later for immunohistochemistry of brain sections.
(B) Example section of immunohistochemistry of TRAP+ cells in the dorsal DG illustrating the distinct blades of the DG: SB and IB. Calibration bar: 40 µm.
(C) Density of TRAP+ GCs in mice after running compared to home cage controls (H). Each group represents mice that ran after variable time intervals following BrdU injections.
(D) Blade specific distribution of TRAP+ cells in the infrapyramidal (IB) and suprapyramidal (SB) blades of the dorsal DG in TRAP2 mice that ran for 4 hours, compared to home cage mice. (IB: home: 42.5 ± 1.43 %, 4 mice; run: 43.9 ± 1.42 %, 33 mice; ns; Mann–Whitney).
(E) Example section from mice labeled for BrdU (green), TRAP+ GCs (red) and endogenous c-Fos (blue) in TRAP2 mice. Calibration bar: 20 µm.
(F) Percentage of BrdU+ cells (Δ 1-14 weeks old) also labeled with TRAP in the dorsal DG of TRAP2 mice that ran for 4 hours, compared to home cage controls (H).
(G) Blade specific distribution of BrdU+ cells in the infrapyramidal (IB) and suprapyramidal (SB) blades of the dorsal DG in TRAP2 mice that ran for 4 hours, compared to home cage mice.

Figure Sup 2: **Description of the TUNL protocol and analysis of TRAP+ GCs in mice not meeting the criterion in the pattern separation task.**

(A) Overview of successive trials in the Shaping, L and LS steps. Mice must complete 30 trials at each step. The shaping phase involves touching the illuminated square to receive a reward. In the L and LS steps, there are in two phases: the sample (S) phase, where mice must touch the single illuminated square on the panel and the choice test (C), where two squares are illuminated: the previously touched square and a new one. Mice must nose poke the new square to receive the reward. In the L phase, trials consist only of L panels only (see Figure S2B – L). In the LS phase, L and S trials are alternated (see Figure S2B for S panels).
(B**)** Recommended stimulus pairs for the TUNL protocol. Large pairs (green) consist of 2 illuminated squares separated by 4 squares that are turned OFF. Small pairs (orange) consist of two illuminated squares separated by 0 to 1 square turned OFF.
(C) Correlation between the performance (= number of days to reach criterion) and the TRAP+ density or TRAP+ distribution in SB (D). Both regression analysis (right tables) show that the slope is not significantly different from zero.
(E) Comparison of TRAP+ distribution in IB and SB of the dorsal DG in mice from the home cage (Home), running (Run), large configuration (L) and large and small separation (LS) groups. In the control groups (Home, Run and L) the TRAP+ cells are predominantly distributed in the SB, with a slight preference for the SB over IB. However, in the high cognitive demand (CD), LS takm the distribution pf TRAP+ cells become more balanced, with a marked preference for the SB (SB >>IB), indicating task-specific modulation of activity across the blades.
(F) Density of c-Fos-labeled GCs in mice undergoing LS compared to control mice engaged in either shaping (Shap) or the Large configuration task only (L) ($H(2) = 11.4$, $p = 0.003$; Kruskal Wallis)(With Dunn post hoc analysis: Shap comparison to L, $p = 0.09$, Shap comparison to LS, $p=0.0008$, L comparison to LS $p = 0.13$).
(G) Percentage of TRAP2 mice reaching the criterion (C) compared to those that did not within 14 days of training (NC).
(H) Density of TRAP+ neurons in mice undergoing LS for mice that reached criterion (LS C) with mice that did not reach 70% criterion within 14 days (LS NC) (LS C: 2563 ± 481 mm^3, 8 mice; LS NC: 2036 ± 305 mm^3, 10 mice; ns; Mann–Whitney).
(I) Blade specific distribution of TRAP+ GCs in the SB and the IB of the dorsal DG (IB: LS C: 34 ± 2.79 %, 8 mice; LS NC : 33.8 ± 2.12 %, 12 mice; ns; Mann–Whitney).
(J) Percentage of TRAP+ cells also birth-dated with BrdU (39 days +/- 1.23) or Edu cells (25 days +/- 1.37 days) in the dorsal DG of TRAP2 mice that reached criterion (C) and those failed (NC)(BrdU: LS C: 0.71 ± 0.333 %, 7 mice; LS NC : 0.822 ± 0.45 %, 6 mice; ns; EdU: LS C: 0.542 ± 0.33 %, 9 mice; LS NC : 0.304 ± 0.16 %, 7 mice; ns; Mann–Whitney).

Figure Sup 3: **Dock10 is not expressed in -positive immature newborn neurons but is expressed in Prox1-positive neurons**

(A) Representative section from a Dock10-cre:Ai9 mouse following tdTomato (tdT), Prox1, and DCX immunohistochemistry in the dorsal DG. Calibration bar: 100 μm.

(B) 20X magnification of the suprapyramidal layer of the dentate gyrus, showing tdTomato (Dock10) in red, Prox1 in green, and DCX in blue. Calibration bar: 100 μm.

(C) tdT (Dock10) labeling. (D) Prox1 (green) labeling. (E) DCX (blue) labeling. Calibration bar: 100 μm.

Citations:

1. Hainmueller, T., and Bartos, M. (2020). Dentate gyrus circuits for encoding, retrieval and discrimination of episodic memories. Nat Rev Neurosci *21*, 153-168. 10.1038/s41583-019-0260-z.
2. Stefanini, F., Kushnir, L., Jimenez, J.C., Jennings, J.H., Woods, N.I., Stuber, G.D., Kheirbek, M.A., Hen, R., and Fusi, S. (2020). A Distributed Neural Code in the Dentate Gyrus and in CA1. Neuron *107*, 703-716 e704. 10.1016/j.neuron.2020.05.022.
3. Hunsaker, M.R., Rosenberg, J.S., and Kesner, R.P. (2008). The role of the dentate gyrus, CA3a,b, and CA3c for detecting spatial and environmental novelty. Hippocampus *18*, 1064-1073. 10.1002/hipo.20464.
4. Leutgeb, J.K., Leutgeb, S., Moser, M.B., and Moser, E.I. (2007). Pattern separation in the dentate gyrus and CA3 of the hippocampus. Science *315*, 961-966. 10.1126/science.1135801.
5. Marr, D. (1969). A theory of cerebellar cortex. J Physiol *202*, 437-470. 10.1113/jphysiol.1969.sp008820.
6. Marr, D. (1971). Simple memory: a theory for archicortex. Philos Trans R Soc Lond B Biol Sci *262*, 23-81. 10.1098/rstb.1971.0078.
7. Rolls, E.T. (2016). Pattern separation, completion, and categorisation in the hippocampus and neocortex. Neurobiol Learn Mem *129*, 4-28. 10.1016/j.nlm.2015.07.008.
8. Borzello, M., Ramirez, S., Treves, A., Lee, I., Scharfman, H., Stark, C., Knierim, J.J., and Rangel, L.M. (2023). Assessments of dentate gyrus function: discoveries and debates. Nat Rev Neurosci *24*, 502-517. 10.1038/s41583-023-00710-z.
9. Amaral, D.G., Scharfman, H.E., and Lavenex, P. (2007). The dentate gyrus: fundamental neuroanatomical organization (dentate gyrus for dummies). Prog Brain Res *163*, 3-22. 10.1016/S0079-6123(07)63001-5.
10. Chawla, M.K., Guzowski, J.F., Ramirez-Amaya, V., Lipa, P., Hoffman, K.L., Marriott, L.K., Worley, P.F., McNaughton, B.L., and Barnes, C.A. (2005). Sparse, environmentally selective expression of Arc RNA in the upper blade of the rodent fascia dentata by brief spatial experience. Hippocampus *15*, 579-586. 10.1002/hipo.20091.
11. Erwin, S.R., Sun, W., Copeland, M., Lindo, S., Spruston, N., and Cembrowski, M.S. (2020). A Sparse, Spatially Biased Subtype of Mature Granule Cell Dominates

Recruitment in Hippocampal-Associated Behaviors. Cell Rep *31*, 107551. 10.1016/j.celrep.2020.107551.

12. Snyder, J.S., Radik, R., Wojtowicz, J.M., and Cameron, H.A. (2009). Anatomical gradients of adult neurogenesis and activity: young neurons in the ventral dentate gyrus are activated by water maze training. Hippocampus *19*, 360-370. 10.1002/hipo.20525.
13. Scharfman, H.E., Sollas, A.L., Smith, K.L., Jackson, M.B., and Goodman, J.H. (2002). Structural and functional asymmetry in the normal and epileptic rat dentate gyrus. J Comp Neurol *454*, 424-439. 10.1002/cne.10449.
14. Altman, J., and Das, G.D. (1965). Autoradiographic and histological evidence of postnatal hippocampal neurogenesis in rats. J Comp Neurol *124*, 319-335. 10.1002/cne.901240303.
15. Kaplan, M.S., and Hinds, J.W. (1977). Neurogenesis in the adult rat: electron microscopic analysis of light radioautographs. Science *197*, 1092-1094. 10.1126/science.887941.
16. Cameron, H.A., Woolley, C.S., McEwen, B.S., and Gould, E. (1993). Differentiation of newly born neurons and glia in the dentate gyrus of the adult rat. Neuroscience *56*, 337-344. 10.1016/0306-4522(93)90335-d.
17. Kempermann, G., Kuhn, H.G., and Gage, F.H. (1997). More hippocampal neurons in adult mice living in an enriched environment. Nature *386*, 493-495. 10.1038/386493a0.
18. Folsz, O., Trouche, S., and Croset, V. (2023). Adult-born neurons add flexibility to hippocampal memories. Front Neurosci *17*, 1128623. 10.3389/fnins.2023.1128623.
19. Dranovsky, A., Picchini, A.M., Moadel, T., Sisti, A.C., Yamada, A., Kimura, S., Leonardo, E.D., and Hen, R. (2011). Experience dictates stem cell fate in the adult hippocampus. Neuron *70*, 908-923. 10.1016/j.neuron.2011.05.022.
20. Jinno, S. (2011). Topographic differences in adult neurogenesis in the mouse hippocampus: a stereology-based study using endogenous markers. Hippocampus *21*, 467-480. 10.1002/hipo.20762.
21. Ramirez-Amaya, V., Marrone, D.F., Gage, F.H., Worley, P.F., and Barnes, C.A. (2006). Integration of new neurons into functional neural networks. J Neurosci *26*, 12237-12241. 10.1523/JNEUROSCI.2195-06.2006.
22. Alves, N.D., Patricio, P., Correia, J.S., Mateus-Pinheiro, A., Machado-Santos, A.R., Loureiro-Campos, E., Morais, M., Bessa, J.M., Sousa, N., and Pinto, L. (2018). Chronic stress targets adult neurogenesis preferentially in the suprapyramidal blade of the rat dorsal dentate gyrus. Brain Struct Funct *223*, 415-428. 10.1007/s00429-017-1490-3.

23. DeNardo, L.A., Liu, C.D., Allen, W.E., Adams, E.L., Friedmann, D., Fu, L., Guenthner, C.J., Tessier-Lavigne, M., and Luo, L. (2019). Temporal evolution of cortical ensembles promoting remote memory retrieval. Nat Neurosci *22*, 460-469. 10.1038/s41593-018-0318-7.
24. Castillon, C., Lunion, S., Desvignes, N., Hanauer, A., Laroche, S., and Poirier, R. (2018). Selective alteration of adult hippocampal neurogenesis and impaired spatial pattern separation performance in the RSK2-deficient mouse model of Coffin-Lowry syndrome. Neurobiol Dis *115*, 69-81. 10.1016/j.nbd.2018.04.007.
25. Chatzi, C., Zhang, Y., Hendricks, W.D., Chen, Y., Schnell, E., Goodman, R.H., and Westbrook, G.L. (2019). Exercise-induced enhancement of synaptic function triggered by the inverse BAR protein, Mtss1L. Elife *8*. 10.7554/eLife.45920.
26. Deng, W., Mayford, M., and Gage, F.H. (2013). Selection of distinct populations of dentate granule cells in response to inputs as a mechanism for pattern separation in mice. Elife *2*, e00312. 10.7554/eLife.00312.
27. Lamothe-Molina, P.J., Franzelin, A., Beck, L., Li, D., Auksutat, L., Fieblinger, T., Laprell, L., Alhbeck, J., Gee, C.E., Kneussel, M., et al. (2022). DeltaFosB accumulation in hippocampal granule cells drives cFos pattern separation during spatial learning. Nat Commun *13*, 6376. 10.1038/s41467-022-33947-w.
28. Talpos, J.C., McTighe, S.M., Dias, R., Saksida, L.M., and Bussey, T.J. (2010). Trial-unique, delayed nonmatching-to-location (TUNL): a novel, highly hippocampus-dependent automated touchscreen test of location memory and pattern separation. Neurobiol Learn Mem *94*, 341-352. 10.1016/j.nlm.2010.07.006.
29. Oomen, C.A., Hvoslef-Eide, M., Heath, C.J., Mar, A.C., Horner, A.E., Bussey, T.J., and Saksida, L.M. (2013). The touchscreen operant platform for testing working memory and pattern separation in rats and mice. Nat Protoc *8*, 2006-2021. 10.1038/nprot.2013.124.
30. Williams, P.A., Larimer, P., Gao, Y., and Strowbridge, B.W. (2007). Semilunar granule cells: glutamatergic neurons in the rat dentate gyrus with axon collaterals in the inner molecular layer. J Neurosci *27*, 13756-13761. 10.1523/JNEUROSCI.4053-07.2007.
31. Pilz, G.A., Carta, S., Stauble, A., Ayaz, A., Jessberger, S., and Helmchen, F. (2016). Functional Imaging of Dentate Granule Cells in the Adult Mouse Hippocampus. J Neurosci *36*, 7407-7414. 10.1523/JNEUROSCI.3065-15.2016.
32. Danielson, N.B., Kaifosh, P., Zaremba, J.D., Lovett-Barron, M., Tsai, J., Denny, C.A., Balough, E.M., Goldberg, A.R., Drew, L.J., Hen, R., et al. (2016). Distinct Contribution of

Adult-Born Hippocampal Granule Cells to Context Encoding. Neuron *90*, 101-112. 10.1016/j.neuron.2016.02.019.

33. Kohara, K., Pignatelli, M., Rivest, A.J., Jung, H.Y., Kitamura, T., Suh, J., Frank, D., Kajikawa, K., Mise, N., Obata, Y., et al. (2014). Cell type-specific genetic and optogenetic tools reveal hippocampal CA2 circuits. Nat Neurosci *17*, 269-279. 10.1038/nn.3614.
34. Nagai, Y., Miyakawa, N., Takuwa, H., Hori, Y., Oyama, K., Ji, B., Takahashi, M., Huang, X.P., Slocum, S.T., DiBerto, J.F., et al. (2020). Deschloroclozapine, a potent and selective chemogenetic actuator enables rapid neuronal and behavioral modulations in mice and monkeys. Nat Neurosci *23*, 1157-1167. 10.1038/s41593-020-0661-3.
35. Ikrar, T., Guo, N., He, K., Besnard, A., Levinson, S., Hill, A., Lee, H.K., Hen, R., Xu, X., and Sahay, A. (2013). Adult neurogenesis modifies excitability of the dentate gyrus. Front Neural Circuits *7*, 204. 10.3389/fncir.2013.00204.
36. Drew, L.J., Kheirbek, M.A., Luna, V.M., Denny, C.A., Cloidt, M.A., Wu, M.V., Jain, S., Scharfman, H.E., and Hen, R. (2016). Activation of local inhibitory circuits in the dentate gyrus by adult-born neurons. Hippocampus *26*, 763-778. 10.1002/hipo.22557.
37. Zhu, H., Aryal, D.K., Olsen, R.H., Urban, D.J., Swearingen, A., Forbes, S., Roth, B.L., and Hochgeschwender, U. (2016). Cre-dependent DREADD (Designer Receptors Exclusively Activated by Designer Drugs) mice. Genesis *54*, 439-446. 10.1002/dvg.22949.
38. Yang, S.M., Alvarez, D.D., and Schinder, A.F. (2015). Reliable Genetic Labeling of Adult-Born Dentate Granule Cells Using Ascl1 CreERT2 and Glast CreERT2 Murine Lines. J Neurosci *35*, 15379-15390. 10.1523/JNEUROSCI.2345-15.2015.
39. Tunc-Ozcan, E., Peng, C.Y., Zhu, Y., Dunlop, S.R., Contractor, A., and Kessler, J.A. (2019). Activating newborn neurons suppresses depression and anxiety-like behaviors. Nat Commun *10*, 3768. 10.1038/s41467-019-11641-8.
40. Lacefield, C.O., Itskov, V., Reardon, T., Hen, R., and Gordon, J.A. (2012). Effects of adult-generated granule cells on coordinated network activity in the dentate gyrus. Hippocampus *22*, 106-116. 10.1002/hipo.20860.
41. Ge, S., Yang, C.H., Hsu, K.S., Ming, G.L., and Song, H. (2007). A critical period for enhanced synaptic plasticity in newly generated neurons of the adult brain. Neuron *54*, 559-566. 10.1016/j.neuron.2007.05.002.
42. Kennedy, W.M., Gonzalez, J.C., Lee, H., Wadiche, J.I., and Overstreet-Wadiche, L. (2024). T-Type Ca(2+) Channels Mediate a Critical Period of Plasticity in Adult-Born Granule Cells. J Neurosci *44*. 10.1523/JNEUROSCI.1503-23.2024.

43. Guzman, S.J., Schlogl, A., Espinoza, C., Zhang, X., Suter, B.A., and Jonas, P. (2021). How connectivity rules and synaptic properties shape the efficacy of pattern separation in the entorhinal cortex-dentate gyrus-CA3 network. Nat Comput Sci *1*, 830-842. 10.1038/s43588-021-00157-1.
44. Besnard, A., and Sahay, A. (2021). Enhancing adult neurogenesis promotes contextual fear memory discrimination and activation of hippocampal-dorsolateral septal circuits. Behav Brain Res *399*, 112917. 10.1016/j.bbr.2020.112917.
45. Berdugo-Vega, G., Lee, C.C., Garthe, A., Kempermann, G., and Calegari, F. (2021). Adult-born neurons promote cognitive flexibility by improving memory precision and indexing. Hippocampus *31*, 1068-1079. 10.1002/hipo.23373.
46. Berdugo-Vega, G., Dhingra, S., and Calegari, F. (2023). Sharpening the blades of the dentate gyrus: how adult-born neurons differentially modulate diverse aspects of hippocampal learning and memory. EMBO J *42*, e113524. 10.15252/embj.2023113524.
47. van Praag, H., Schinder, A.F., Christie, B.R., Toni, N., Palmer, T.D., and Gage, F.H. (2002). Functional neurogenesis in the adult hippocampus. Nature *415*, 1030-1034. 10.1038/4151030a.
48. Zhao, C., Teng, E.M., Summers, R.G., Jr., Ming, G.L., and Gage, F.H. (2006). Distinct morphological stages of dentate granule neuron maturation in the adult mouse hippocampus. J Neurosci *26*, 3-11. 10.1523/JNEUROSCI.3648-05.2006.
49. Toni, N., Teng, E.M., Bushong, E.A., Aimone, J.B., Zhao, C., Consiglio, A., van Praag, H., Martone, M.E., Ellisman, M.H., and Gage, F.H. (2007). Synapse formation on neurons born in the adult hippocampus. Nat Neurosci *10*, 727-734. 10.1038/nn1908.
50. Temprana, S.G., Mongiat, L.A., Yang, S.M., Trinchero, M.F., Alvarez, D.D., Kropff, E., Giacomini, D., Beltramone, N., Lanuza, G.M., and Schinder, A.F. (2015). Delayed coupling to feedback inhibition during a critical period for the integration of adult-born granule cells. Neuron *85*, 116-130. 10.1016/j.neuron.2014.11.023.
51. Johnston, S.T., Shtrahman, M., Parylak, S., Goncalves, J.T., and Gage, F.H. (2016). Paradox of pattern separation and adult neurogenesis: A dual role for new neurons balancing memory resolution and robustness. Neurobiol Learn Mem *129*, 60-68. 10.1016/j.nlm.2015.10.013.
52. Dieni, C.V., Gonzalez, J.C., and Overstreet-Wadiche, L. (2019). Multifaceted circuit functions of adult-born neurons. F1000Res *8*. 10.12688/f1000research.20642.1.
53. Luna, V.M., Anacker, C., Burghardt, N.S., Khandaker, H., Andreu, V., Millette, A., Leary, P., Ravenelle, R., Jimenez, J.C., Mastrodonato, A., et al. (2019). Adult-born hippocampal

neurons bidirectionally modulate entorhinal inputs into the dentate gyrus. Science *364*, 578-583. 10.1126/science.aat8789.

54. Tuncdemir, S.N., Lacefield, C.O., and Hen, R. (2019). Contributions of adult neurogenesis to dentate gyrus network activity and computations. Behav Brain Res *374*, 112112. 10.1016/j.bbr.2019.112112.

55. Clelland, C.D., Choi, M., Romberg, C., Clemenson, G.D., Jr., Fragniere, A., Tyers, P., Jessberger, S., Saksida, L.M., Barker, R.A., Gage, F.H., and Bussey, T.J. (2009). A functional role for adult hippocampal neurogenesis in spatial pattern separation. Science *325*, 210-213. 10.1126/science.1173215.

56. Sahay, A., Scobie, K.N., Hill, A.S., O'Carroll, C.M., Kheirbek, M.A., Burghardt, N.S., Fenton, A.A., Dranovsky, A., and Hen, R. (2011). Increasing adult hippocampal neurogenesis is sufficient to improve pattern separation. Nature *472*, 466-470. 10.1038/nature09817.

57. Creer, D.J., Romberg, C., Saksida, L.M., van Praag, H., and Bussey, T.J. (2010). Running enhances spatial pattern separation in mice. Proc Natl Acad Sci U S A *107*, 2367-2372. 10.1073/pnas.0911725107.

58. Kim, E.J., Ables, J.L., Dickel, L.K., Eisch, A.J., and Johnson, J.E. (2011). Ascl1 (Mash1) defines cells with long-term neurogenic potential in subgranular and subventricular zones in adult mouse brain. PLoS One *6*, e18472. 10.1371/journal.pone.0018472.

59. Castillon, C., Gonzalez, L., Domenichini, F., Guyon, S., Da Silva, K., Durand, C., Lestaevel, P., Vaillend, C., Laroche, S., Barnier, J.V., and Poirier, R. (2020). The intellectual disability PAK3 R67C mutation impacts cognitive functions and adult hippocampal neurogenesis. Hum Mol Genet *29*, 1950-1968. 10.1093/hmg/ddz296.

60. Sloviter, R.S., Dichter, M.A., Rachinsky, T.L., Dean, E., Goodman, J.H., Sollas, A.L., and Martin, D.L. (1996). Basal expression and induction of glutamate decarboxylase GABA in excitatory granule cells of the rat and monkey hippocampal dentate gyrus. The Journal of Comparative Neurology *373*, 593-618. 10.1002/(sici)1096-9861(19960930)373:4<593::Aid-cne8>3.0.Co;2-x.

61. Perederiy, J.V., Luikart, B.W., Washburn, E.K., Schnell, E., and Westbrook, G.L. (2013). Neural injury alters proliferation and integration of adult-generated neurons in the dentate gyrus. J Neurosci *33*, 4754-4767. 10.1523/JNEUROSCI.4785-12.2013.

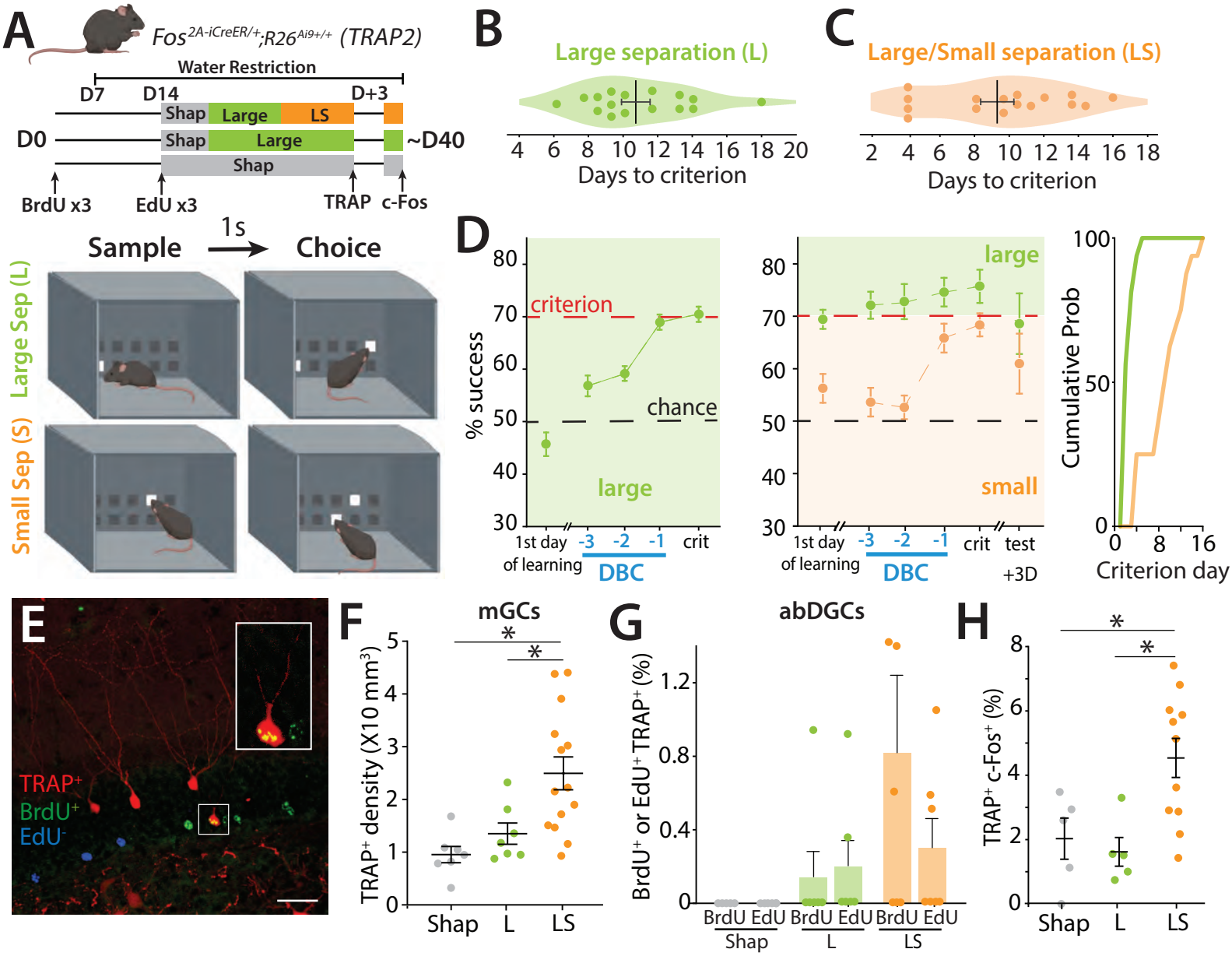
A
Fos2A-iCreER/+;R26Ai9+/+ (TRAP2)
Water Restriction
D7
D14
D+3
D0
Shap
Large
LS
~D40
BrdU x3
EdU x3
TRAP
c-Fos
Sample
1s
Choice
Large Sep (L)
Small Sep (S)
B
Large separation (L)
Days to criterion
C
Large/Small separation (LS)
Days to criterion
D
% success
criterion
chance
large
1st day of learning
DBC
crit
small
test
+3D
Cumulative Prob
Criterion day
E
TRAP+
BrdU+
EdU-
F
mGCs
TRAP+ density (X10 mm3)
Shap
L
LS
G
abDGCs
BrdU+ or EdU+ TRAP+ (%)
BrdU EdU
H
TRAP+ c-Fos+ (%)

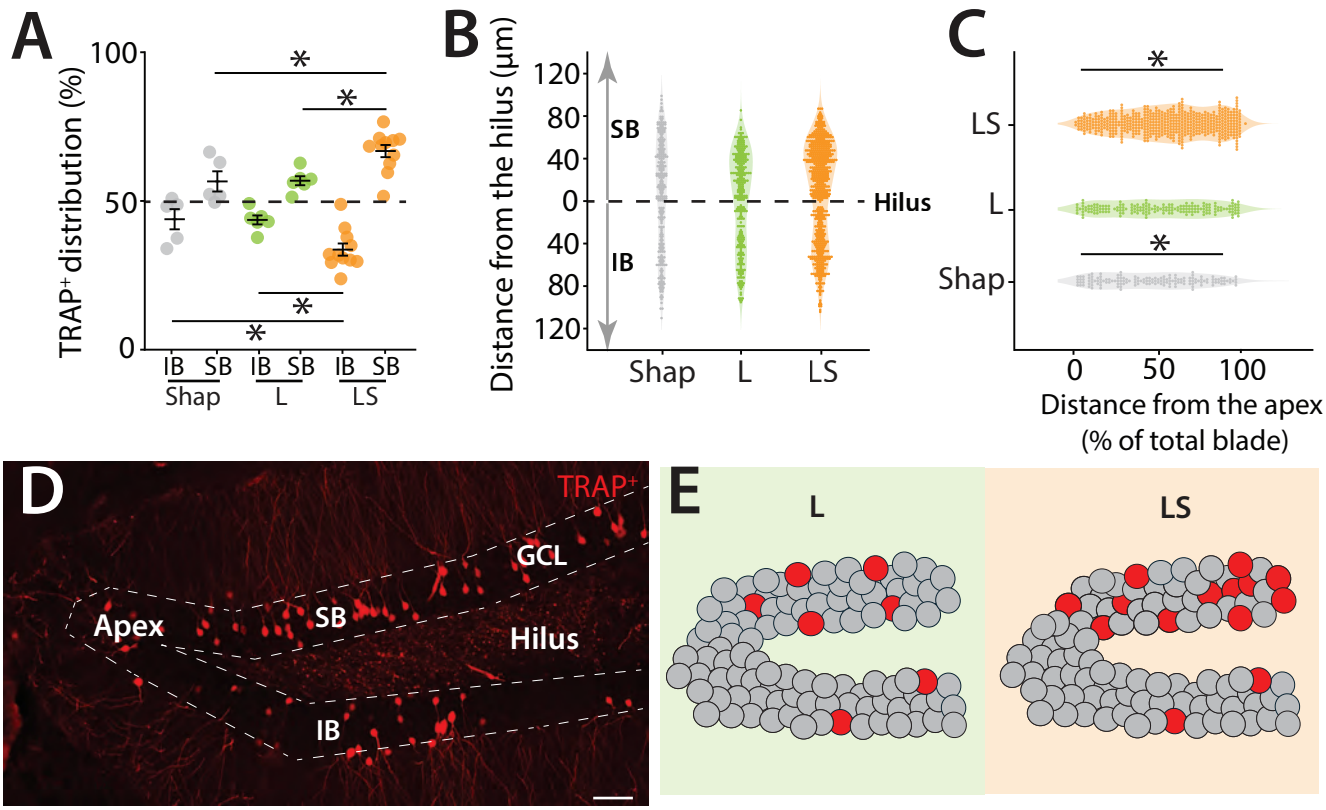
A
TRAP+ distribution (%)
100
50
0
IB SB IB SB IB SB
Shap L LS
B
Distance from the hilus (µm)
120
80
40
0
40
80
120
SB
IB
Hilus
Shap L LS
C
LS
L
Shap
0 50 100
Distance from the apex
(% of total blade)
D
TRAP+
GCL
Apex
SB
Hilus
IB
E
L
LS

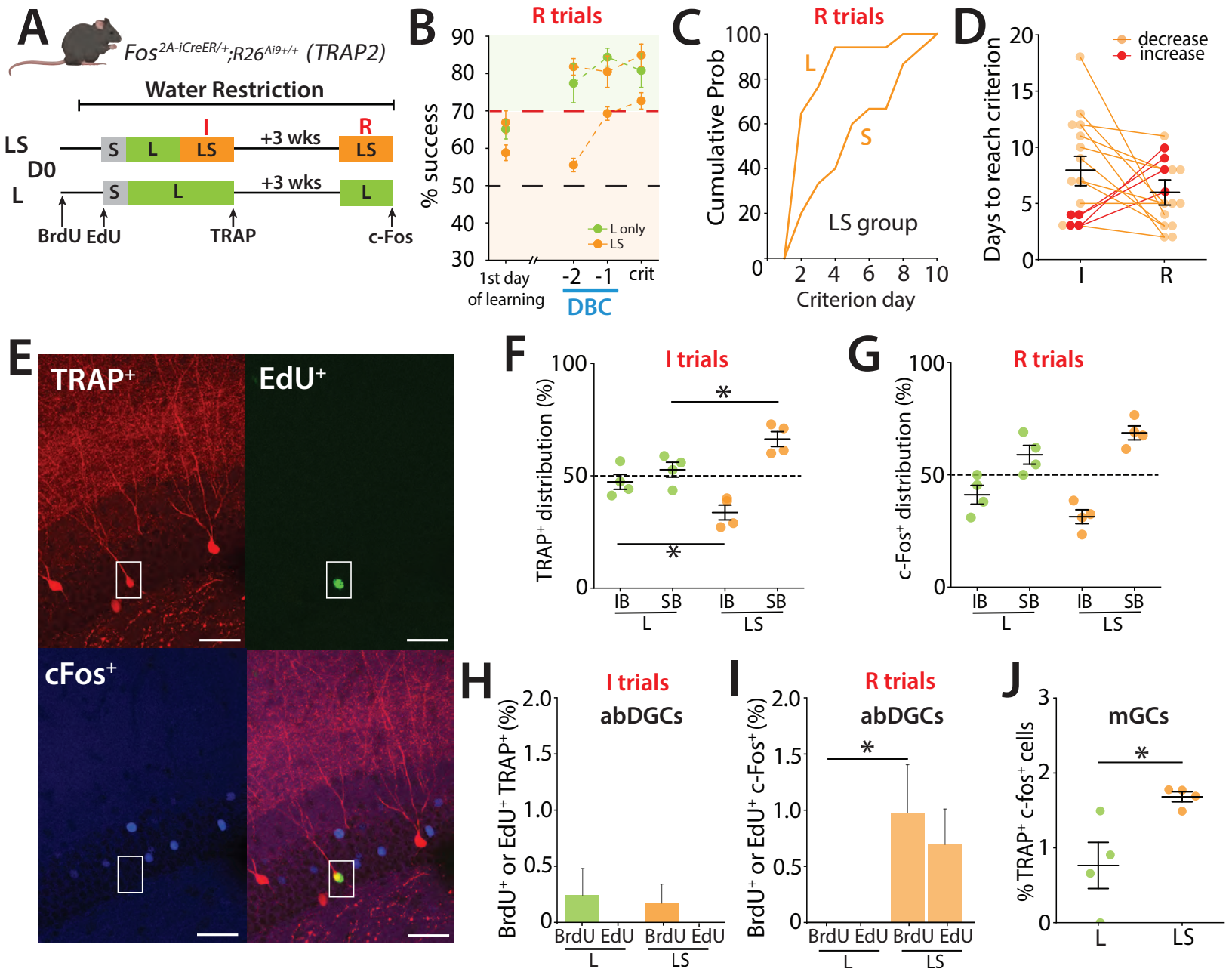
A
Fos2A-iCreER/+;R26Ai9+/+ (TRAP2)
Water Restriction
LS
D0
L
S
L
LS
I
+3 wks
R
LS
S
L
+3 wks
L
BrdU EdU
TRAP
c-Fos
B
R trials
% success
L only
LS
1st day of learning
-2
-1
crit
DBC
C
R trials
Cumulative Prob
L
S
LS group
Criterion day
D
decrease
increase
Days to reach criterion
I
R
E
TRAP+
EdU+
cFos+
F
I trials
TRAP+ distribution (%)
IB
SB
IB
SB
L
LS
G
R trials
c-Fos+ distribution (%)
IB
SB
IB
SB
L
LS
H
I trials
abDGCs
BrdU+ or EdU+ TRAP+ (%)
BrdU EdU
BrdU EdU
L
LS
I
R trials
abDGCs
BrdU+ or EdU+ c-Fos+ (%)
BrdU EdU
BrdU EdU
L
LS
J
mGCs
% TRAP+ c-fos+ cells
L
LS

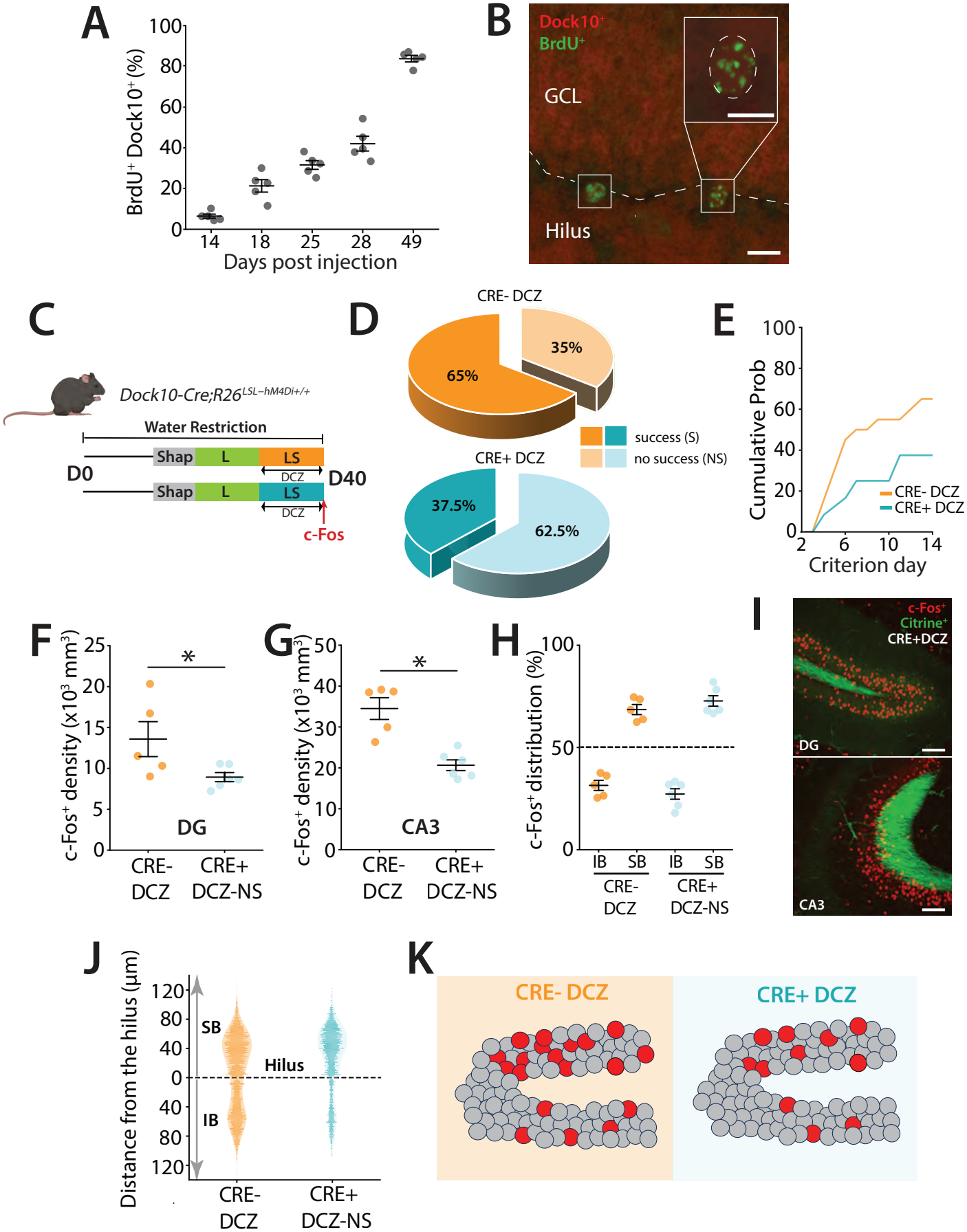
A
BrdU+ Dock10+ (%)
100
80
60
40
20
0
14
18
25
28
49
Days post injection
B
Dock10+
BrdU+
GCL
Hilus
C
Dock10-Cre;R26LSL−hM4Di+/+
Water Restriction
Shap
L
LS
DCZ
D0
D40
c-Fos
D
CRE- DCZ
65%
35%
CRE+ DCZ
37.5%
62.5%
success (S)
no success (NS)
E
Cumulative Prob
Criterion day
CRE- DCZ
CRE+ DCZ
F
c-Fos+ density (x10³ mm³)
DG
CRE- DCZ
CRE+ DCZ-NS
G
CA3
H
c-Fos+ distribution (%)
IB
SB
I
c-Fos+
Citrine+
CRE+DCZ
DG
CA3
J
Distance from the hilus (µm)
SB
IB
Hilus
K
CRE- DCZ
CRE+ DCZ

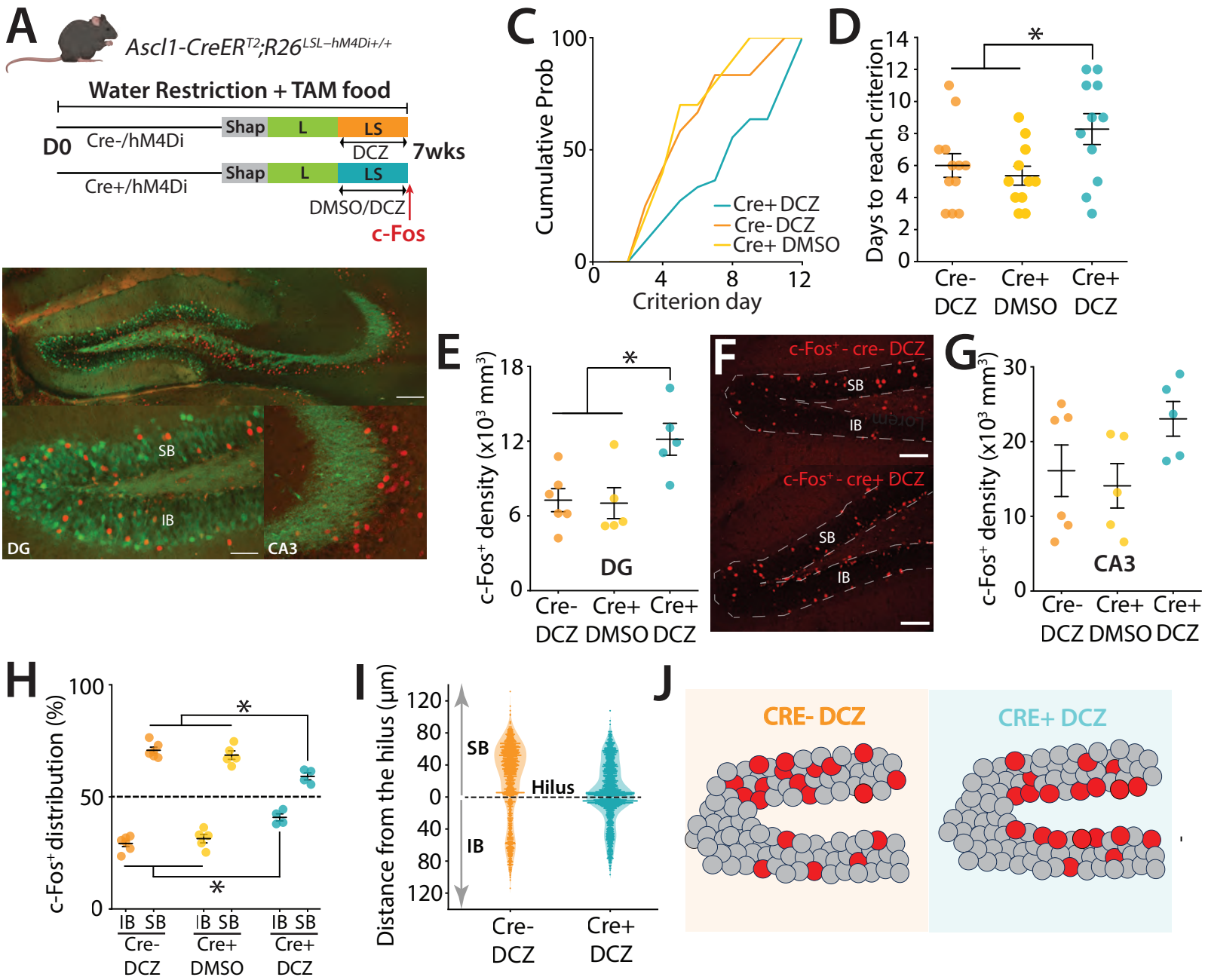
A
Ascl1-CreER^{T2};R26$^{LSL-hM4Di+/+}$
Water Restriction + TAM food
D0
Cre-/hM4Di
Shap
L
LS
DCZ
7wks
Cre+/hM4Di
Shap
L
LS
DMSO/DCZ
c-Fos
SB
IB
DG
CA3
C
Cumulative Prob
Criterion day
Cre+ DCZ
Cre- DCZ
Cre+ DMSO
D
Days to reach criterion
Cre- DCZ
Cre+ DMSO
Cre+ DCZ
E
c-Fos+ density (x10^3 mm^3)
DG
Cre- DCZ
Cre+ DMSO
Cre+ DCZ
F
c-Fos+ - cre- DCZ
SB
IB
c-Fos+ - cre+ DCZ
SB
IB
G
c-Fos+ density (x10^3 mm^3)
CA3
Cre- DCZ
Cre+ DMSO
Cre+ DCZ
H
c-Fos+ distribution (%)
IB SB
Cre- DCZ
IB SB
Cre+ DMSO
IB SB
Cre+ DCZ
I
Distance from the hilus (µm)
SB
Hilus
IB
Cre- DCZ
Cre+ DCZ
J
CRE- DCZ
CRE+ DCZ

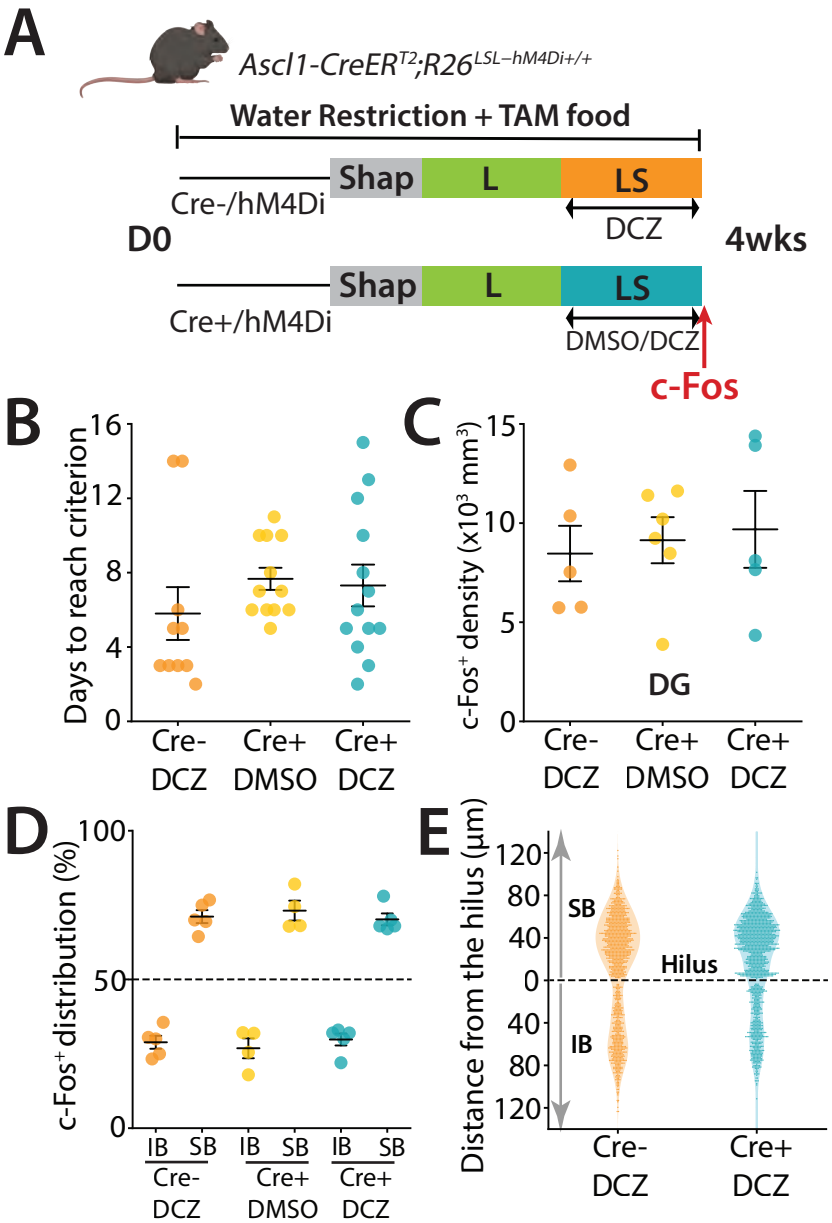
A
Ascl1-CreER^{T2};R26$^{LSL-hM4Di+/+}$
Water Restriction + TAM food
Shap
L
LS
Cre-/hM4Di
DCZ
D0
4wks
Shap
L
LS
Cre+/hM4Di
DMSO/DCZ
c-Fos
B
Days to reach criterion
16
12
8
4
0
Cre-
DCZ
Cre+
DMSO
Cre+
DCZ
C
c-Fos$^+$ density (x10^3 mm^3)
15
10
5
0
DG
Cre-
DCZ
Cre+
DMSO
Cre+
DCZ
D
c-Fos$^+$ distribution (%)
100
50
0
IB
SB
IB
SB
IB
SB
Cre-
DCZ
Cre+
DMSO
Cre+
DCZ
E
Distance from the hilus (µm)
120
80
40
0
40
80
120
SB
Hilus
IB
Cre-
DCZ
Cre+
DCZ